2008

Surface temperature mapping of the University of Northern Iowa campus using high resolution thermal infrared aerial imagery

Alexander Savelyev
University of Northern Iowa

SURFACE TEMPERATURE MAPPING OF THE UNIVERSITY OF NORTHERN IOWA CAMPUS USING HIGH RESOLUTION THERMAL INFRARED AERIAL IMAGERY

An Abstract of Thesis

Submitted

in Partial Fulfillment

of the Requirements for the Degree

Master of Arts

Alexander Savelyev

University of Northern Iowa

December 2008

ABSTRACT

The goal of this study was to produce and analyze a heat loss map of the University of the Northern Iowa campus using thermal infrared remote sensing data. Aerial data with the spatial resolution of 0.29m and radiometric resolution of 14 bit was collected. A model for the pixel to radiance and temperature conversion was developed with its parameters estimated with an R^2 of 0.78. Temperature imagery was shown to be consistent over the time of the survey and accurate to within 1.2°C. The temperature map then was used to assess the conditions of the rooftops and steam pipelines present in the study area. Analysis of the temperature map revealed a number of rooftops that may be subject to the insulation improvement. Several hot spots were also identified as faults in the insulation of steam pipelines. High-resolution thermal infrared imagery proved to be a highly effective tool for precise heat anomaly detection. Data obtained in this survey is now being used by Facilities Planning department of the University of the Northern Iowa as part of the effective maintenance of buildings and grounds.

SURFACE TEMPERATURE MAPPING OF THE UNIVERSITY OF NORTHERN IOWA CAMPUS USING HIGH RESOLUTION THERMAL INFRARED AERIAL IMAGERY

A Thesis

Submitted

in Partial Fulfillment

of the Requirements for the Degree

Master of Arts

Alexander Savelyev

University of Northern Iowa

December 2008

This Study by: Alexander Savelyev

Entitled: SURFACE TEMPERATURE MAPPING OF THE UNIVERSITY OF NORTHERN IOWA CAMPUS USING HIGH RESOLUTION THERMAL INFRARED AERIAL IMAGERY

has been approved as meeting the thesis requirement for the

Degree of Master of Arts

11-07-08	
Date	Dr. Ramanathan Sugumaran, Chair, Thesis Committee
11-7-08	
Date	Dr. Patrick Pease, Thesis Committee Member
11-7-08	
Date	Dr. David W. May, Thesis Committee Member
11/24/08	
Date	Dr. Sue A. Joseph, Interim Dean, Graduate College

ACKNOWLEDGMENTS

I would like to acknowledge and express my sincere gratitude to NASA for providing generous funding for this project; my thesis committee members - Dr. Sugumaran, Dr. Patrick Pease and Dr. David W. May, for their patience and guidance; John DeGroote, Matthew Voss and the rest of the GeoTREE staff for their constant help; Facilities Planning department for their invaluable help with data analysis; Scott Larson and Adam Lee for their help with the data collection and processing; Jane Gillen for taking care of numerous small problems that would have otherwise slowed this project down.

TABLE OF CONTENTS

PAGE

LIST OF TABLES

LIST OF FIGURES

CHAPTER 1

INTRODUCTION

Heat loss detection is an important aspect of infrastructure maintenance. With fuel prices rising and ecology concerns gaining voice, managers and engineers face the problem of heat loss reduction. One of the common ways to improve energy efficiency is to identify temperature anomalies ("hot spots") in the existing infrastructure. Defects in building insulation, leakage in underground pipelines, and general insulation deterioration are good examples of heat loss sources. Thermal radiation is not perceived by the human eye, which complicates the process of hot spot detection. Thermal remote sensing makes thermal radiation visible, which makes it an excellent solution to the problem of locating hot spots. Thermal infrared sensors can be handheld or fixed on a platform such as an airplane, a satellite or a car. Each of these platforms has its own advantages and disadvantages.

Traditionally, heat loss detection is performed with ground-based thermal sensors. A trained operator with a handheld infrared sensor performs thorough analysis of the object of interest. This approach has a number of benefits, such as high spatial resolution, flexibility and fast deployment (Titman, 2001). Objects of survey can be manually put under the desired workload to maximize thermal contrast. The main drawback of this approach is its extensive nature - with the region of study growing in size, exponentially more time is consumed. Another negative point is that manual survey is discontinuous by nature. The state of the large infrastructure system cannot be expected to stay the same

over long periods of time. Finally, the report from a ground-based survey, however detailed, cannot be easily incorporated into the GIS system for automated analysis. These are main reasons why ground-based infrared surveys are not used for large projects.

Satellite and aerial-based thermal remote sensing is better suited for large areas. Thermal imagery can easily be georeferenced, imported into any GIS system and prepared for automated analysis. As described in MacKay (1984), the instantaneous nature of thermal images is a desirable quality.

Satellite systems have a number of advantages: they offer vast coverage, collect imagery at regular intervals and at low cost. On the other hand, satellite imagery is not available at request because the orbital path is not easily adjustable. Also, thick layers of atmosphere results in a large amount of atmospherical noise, and the combination of limited pixel dwell-time and low level of signal in the infrared part of the spectrum only allows for spatial resolution of 60m or worse (60m for Landsat, Band #6 and 90m for Aster, Bands #10 to 14, according to NASA specifications). Finally, sun-synchronous satellites (such as Aster and Landsat) are not suitable for precise hot spot analysis - re-emitted and reflected solar radiation hides small variations of temperature.

Aerial imagery has a significantly lower level of atmospherical influence compared to satellite systems, it can be acquired on request (at any time of day and night) and with exceptionally high spatial resolution. Several papers have demonstrated that aerial imagery can produce temperature measurements accurate to within 0.6-1.7°C (Kulacki, Mintzer, & Winget, 1981; Schott, Biegel, & Wilkinson, 1982; Schott & Wilkinson, 1981). A number of drawbacks, such as long deployment time (the plane

needs to travel to the place of survey) and relatively high cost (costs of $200,000 for bigger projects are not unusual, see Anderson and Baker (1987) for an example) may become a barrier for smaller projects. However, the advantages of aerial imagery make it ideal for on-demand high-resolution thermal infrared surveys.

An overview of existing heat loss studies (both ground-, aerial- and satellite-based) with a list of analysis techniques is presented in the literature review section.

1.1 Research Goals and Objectives

The main goal of this study was to produce and analyze a heat loss map of the University of the Northern Iowa campus using thermal infrared remote sensing data. This broad task was further divided into three separate objectives.

The first objective was to produce high-quality thermal infrared imagery for the area of the campus. This includes obtaining raw data from the sensor, converting raw data into the shape of digital number (DN) imagery, preprocessing DN imagery, and then georeferencing and mosaicing separate images into the DN mosaic. Digital number imagery corresponds to the voltage levels as perceived by the sensor – it shows neither temperature, nor the radiance of the object of interest. In order to transform digital numbers to radiance and temperature values, some additional steps must be made. A mathematical model for the DN to radiance and temperature conversion should be developed, with its parameters estimated from the combination of aerial and ground level data. Some accuracy assessment should also be performed.

The second objective was to locate and explain the hot spots by analyzing the thermal infrared imagery. This includes involving the knowledge of the local Facilities

Planning department to explain the hot spots as fully as possible. Given that people responsible for the on-campus infrastructure become aware of the existence of the hot spots, we hope that this study would benefit the entire campus community. This would solve the problem of data dissemination and interpretation.

Finally, given that this study is using equipment and technology superior to that found in earlier studies, the third objective was to assess the benefits of using:

- thermal infrared data with higher spatial and radiometrical resolution
- modern image processing techniques, such as data overlay and contrast enhancement
- GIS data analysis tools.

Given these objectives, this project will both have practical and theoretical purposes. The practical part of the project – to produce and analyze a thermal infrared map of the campus – corresponds to the main goal. High spatial and radiometrical resolution of the imagery, fully digital image-processing framework and an attempt to perform GIS-based analysis would also differentiate this survey from other papers on aerial based thermal infrared thermography, therefore adding to its theoretical value.

CHAPTER 2

LITERATURE REVIEW

2.1 Introduction

Thermal remote sensing uses infrared radiation (IR) that belongs between the wavelengths of the visible light and microwaves. This range is commonly defined as 0.75-1000 μm, with further division into categories such as "near-infrared" and "far-infrared," depending on the classification. Thermal remote sensing utilizes this part of the electro-magnetic spectrum as its main data carrier. In order to understand the methodology of this research, it is important to have a good grasp of primary components of any thermal remote sensing survey.

The literature review is divided into 7 sections:

- Principles of thermal remote sensing
- Quantitative thermal remote sensing
- Atmospherical influence
- Environmental factors affecting data acquisition
- Qualitative thermal remote sensing
- Objects of interest
- Summary

Section 2.2 of the literature review describes fundamental laws of physics that form the theoretical basement of the thermal remote sensing. These laws describe the relationship between the infrared radiation from an object and its temperature and emissivity factor. Quantitative thermal remote sensing, that is described in the Section 2.3, is a branch of thermal remote sensing that relies on the application of these theoretical principles. All sorts of numerical models that perform the conversion of infrared radiation levels into temperature fall under this term.

Sections 2.4 and 2.5 describe factors that affect precise quantitative analysis. Section 2.4 ("Atmospherical Influence") explains the influence of the column of air between the sensor and the object of interest. Exact form of this influence can be defined empirically or predicted by atmospherical models. Section 2.5 ("Environmental Factors Affecting the Survey") explains a number of smaller factors, described simultaneously as the environmental noise, that also contributes errors to the quantification process. Reflected and re-emitted radiation from clear sky and neighboring objects belongs to this category.

Section 2.6 of the literature review ("Qualitative Thermal Remote Sensing") provides an insight into qualitative surveys, which omit quantitative analysis completely. In this case, raw thermal imagery is used directly by a skilled interpreter. This approach is significantly simpler than quantitative thermal remote sensing, but is now considered obsolete due to the widespread use of GIS and digital image processing.

Section 2.7 ("Objects of Interest") describes important properties of the objects of study that are specific for thermal remote sensing. These properties apply equally to

quantitative and qualitative methodologies, and include factors such as microclimate, presence of trapped moisture, ventilated attics and sloped roofs.

Section 2.8 presents a short summary of this literature review, with the main requirements for the surveys of this type outlined.

2.2 Principles of Thermal Remote Sensing

The underlying principles that are used throughout all the existing projects are fairly simple. All objects with a temperature above absolute zero emit electromagnetic radiation. This form of radiation is also known as thermal radiation, because it is due to the temperature of the object. The total rate of thermal radiation is described by the Stefan-Boltzmann Law,

$$j^* = \sigma T^4$$

where σ is the Stefan–Boltzmann constant ($5.670400 \cdot 10^{-8}$ $W \cdot m^{-2} \cdot K^{-4}$) and T is the temperature in degrees of Kelvin. The wavelength of maximum emission is described by the Wien's Displacement Law,

$$\lambda_{max} = \frac{b}{T}$$

where b is the Wien's displacement constant ($2.8977685 \cdot 10^{-3}$ $m \cdot K$) and T is the temperature in degrees of Kelvin. The exact form of the emitted spectrum is given by the Planck's Law,

$$I(\lambda,T)=\frac{2hc^2}{\lambda^5}\frac{1}{e^{\frac{hc}{\lambda kT}}-1}$$

where h is the Planck constant ($6.62606893\cdot10^{-34}$ J·s), k is the Boltzmann constant ($1.3806504\cdot10^{-23}$ J·K^{-1}) and c is the speed of light in vacuum (299792458 m·s^{-1}), T is the temperature in degrees of Kelvin and λ is the wavelength of interest.

It is important to understand that these equations describe the behavior of an ideal object – black body, which can be described by its emissivity factor of 1 (or its reflectivity factor of 0, because these two factors are tied by an inverse relationship). For real objects, however, it is necessary to account for the objects' emissivity being different from unity.

2.3 Quantitative Thermal Remote Sensing

With theoretical principles of thermal remote sensing in mind, it is possible to create a number of models that are used in quantitative research. There are three possible "states" for the quantitative data: pixel values (raw data from the sensor, describing a given object), radiance (measure of the thermal radiation flux from a given object) and temperature (temperature of a given object).

When the incoming flux of infrared energy from the object reaches the sensor, it is first converted to electrical current. This current is later processed by the sensor's electronics to obtain pixel values. The exact form of this two-step processing is only known to the manufacturer of the sensor. Colcord and Asce (1978) performed an inquiry into the mechanism of the first part of this conversion, using the type of the infrared

sensor as a starting point. Such inquiries have little practical importance, because the type of the sensor alone does not determine the conversion of voltage to pixel values.

Pixel values can be used to perform relative analysis of temperature distribution on the surface of the object. If absolute temperature values are required, there are two courses of action. First approach is to convert pixel values to radiance, then use the radiance values as an input to the Planck's formula. Schott and Wilkinson (1981) and Schott et al. (1982) illustrate this approach. Second approach, utilized by Kulacki et al. (1981), MacKay (1984) and Tanis and Sampson (1977) is to convert pixel values into temperature directly. Strictly speaking, the latter conversion may provide results identical to the Planck's formula, if the numerical model accounts for the Planck's Law complexity. None of the papers utilizing second approach provide a justification of their conversion algorithms.

Independent of conversion method used, calibration data for the sensor can be gathered on board of the plane (using a laboratory black body as a reference, as it was done by Brown, Cihlar, and Teillet, 1981, MacKay, 1984 and Tanis and Sampson, 1977), on the ground (using thermocouples, as in Treado and Burch, 1981) or both (Kulacki et al., 1981; Schott & Wilkinson, 1981; Schott et al., 1982). If the temperature (or radiance) of a certain object is known at the ground and at the sensor level, it is possible to measure the influence of the emissivity and background noise. If this is not the case, errors in the conversion models cannot be precisely estimated.

As it was mentioned before, adjustments should be made for the emissivity of samples and objects of interest. The problem of estimating emissivity directly from the

remote sensing data is not a new one. Satellite-based studies that, due to the vast nature of satellite imagery, cannot afford to sample the emissivity on the ground level have developed a number of techniques for direct extraction of the emissivity values.

Becker and Li (1990) utilized a modified form of the Planck's Law in the attempt to construct channel-specific indices which would depend on the emissivity values directly, giving birth to the temperature-independent thermal infrared spectral indices (TISI) method of emissivity assessment. Watson (1992) made the assumption that, given two different channels, the changes in the temperature of the object of interest affect the ratio of emissivities significantly less than they affect emissivities on their own. This assumption is the base for the spectral ratio technique. Other methods, such as normalized emissivity method (NEM) by Gillespie (1985), alpha-residual method, developed by Kealy and Gabell (1990) and enhanced by Gu and Gillespie (2000), as well as the temperature emissivity separation (TES) method by Gillespie et al. (1998) are also available.

All of the techniques mentioned above have one common requirement - data from at least two different spectral channels must be present. Most of the aerial thermal infrared surveys, however, are limited to the single-band data, and different techniques of emissivity correction were considered. Most such papers (Kulacki et al., 1981; Schott& Wilkinson, 1981; Tanis & Sampson, 1977; Treado & Burch, 1981) use pre-compiled emissivity tables that exist for a wide range of materials. Is it important to mention that for some types of materials (such as tar and asphalt) variations in level of emissivity are close to 0%, whereas for different sorts of concrete this discrepancy may reach 5%, and

for different sorts of brick it may reach as high as 20%. To avoid this uncertainty, Brown et al. (1981) and Schott et al. (1982) create their own emissivity tables. Schott and Wilkinson (1981) illustrate a combined approach – in this paper emissivity tables are used together with questionnaire data, describing the exact type of material used.

2.4 Atmospherical Influence

When working outside the laboratory setup, it is necessary to account for the atmospherical influence - the air column that lies between the sensor and the object is both emitting and absorbing thermal radiation. There are two main ways to account for atmospherical effects.

The first scenario involves explicit correction for atmospherical effects. A review of literature on the satellite thermal infrared imaging shows that a number of techniques have been developed over time.

An example is the split-window technique (SWT), which relies on the fact that thermal energy is absorbed differently in adjacent channels to determine the influence of the atmosphere. The exact formulas used by this technique vary significantly, depending on the assumptions made by the user, but the main idea as well as general limitations of the SWT were outlined by McMillin (1975) and Kidder and Vonder Haar (1995). Independent on the formula used, this method requires observations in multiple channels.

Another well-known technique is the multi-angle method, which is using the fact that the length of the atmospherical path to the object depends on the angle of view (Prata, 1993). The main requirement of this technique is that the difference between atmospherical paths to the object of interest must be significant.

So called single-channel method of atmospherical correction does not require neither multi-channel, nor multi-angular observations. This method is using one of numerous Radiative Transfer Models (RTM), such as a very well known moderate resolution atmospheric transmission (MODTRAN) program. RTMs allow estimating the absorption and emission of the air column as a function of its height, temperature, pressure and humidity gradients (Ottle & Vidal-Madjar, 1992). Complex models require more parameters, but give better results for a broad range of conditions. RTMs are widely used for satellite imaging, such as in Kumar, Minnet, Podesta, and Evans (2003) and Kumar, Minnet, Podesta, Evans, and Kilpatrick (2000).

The second scenario can be illustrated by the works of Schott and Wilkinson (1981) and Schott et al. (1982). These surveys utilize ad-hoc atmospherical correction models instead of well-defined RTMs. Such models are based on the presence of ground-level radiance estimated, which, coupled with the on-plane measurements, allow to estimate the influence of the column of air between the sensor and the object of interest. Aerial surveys that utilize any sort of atmospherical correction are rare, and most papers do not account for atmospherical effects at all. This topic is either omitted, or, as in the case of Brown et al. (1981), such models are deemed useless because of low flight attitude. None of the papers that omit atmospherical correction present a justification for doing so.

As it was mentioned before, all atmospherical models require precise meteorological control during the time of the survey. Most quantitative aerial surveys (Birnie, Rithie, Stove, & Adams, 1984; Brown et al., 1981; Kulacki et al., 1981; Schott &

Wilkinson, 1981; Schott et al., 1982; Treado & Burch, 1981) perform continuous monitoring of air temperature, humidity, wind speed and direction for a number of locations, regardless of whether they use any sort of RTM or not. None of them, however, go beyond ground level data collection.

2.5 Environmental Factors Affecting Data Acquisition

One of the most important factors that affect temperature values of the objects of interest is environmental noise. It can be divided in two categories – microclimate noise and surface reflection and re-emission.

Microclimate is important for two reasons. First is convective heat loss, which is a function of wind speed and direction. Treado and Burch (1981) found it to be one of the most important noise factors for the sloped rooftops analysis. Second reason is moisture, which might be represented by dew or fog formation. As Colcord and Asce (1978) demonstrate, local moisture formations significantly warp measurements and interpretation. Local air mass migration may result in thermal shades, as in Birnie et al. (1984), or, on the contrary, abnormal heat islands, as in Voogt and Oke (2003).

Surface reflection and re-emission is another source of noise. Reflected sky radiation is routinely mentioned in qualitative surveys and corrected for in quantitative papers. Temporal variations in incoming sky radiation are shown by Treado and Burch (1981) to raise surface temperatures by as much as 3°C. Sky temperature (or downwelling radiation) is usually measured directly. In case direct measurements are not available, a number of approximation techniques can be applied, such as the formula proposed by Swinbank (1963). Nowak (1989) demonstrates that complex geometry of the

object of study will significantly increase the error of unsophisticated clear-sky radiance formulas. Reflection of background objects might also introduce significant amounts of noise in case pitched rooftops with wide view factor are present. As with sky radiation, background radiation is routinely corrected for in most papers.

2.6 Qualitative Thermal Remote Sensing

A number of surveys proved to be fruitful without any quantitative analysis done. For Anderson and Baker (1987) and Birnie et al. (1984), pixel values alone allowed estimating relative level of insulation in nearby building. In case of Baraniak and Williams (1981), ground-based survey, combined with intelligent data dissemination stage, shows exceptional results in determining the sources of heat loss. Pipelines survey described by MacKay (1984) is an example of cooperation with local engineers.

Remote sensing approach allows making an instantaneous snapshot of many individual locations under similar workload and atmospherical conditions. When coupled with local knowledge (either from hired personnel or from data dissemination stage), qualitative survey might be a success. If local knowledge is unavailable, qualitative analysis is shown by Schott et al. (1982) to be at least 30% less precise than quantitative approach.

2.7 Objects of Interest

Objects of interest include the surfaces that exhibit the most substantial part of the heat loss. All papers focus on different aspects of rooftops, walls and pipelines. It is usually the insulation deficiencies that are of the biggest interest. Insulation deterioration

and overall insulation levels are also frequently analyzed. With only three main objects of interest, however, there is a large number of smaller factors that define the survey.

2.7.1 Rooftops

Some papers are dedicated entirely to the analysis of the heat loss from flat rooftops. In case of Anderson and Baker (1987), this is explained by the region of study – mostly industrial buildings with flat rooftops are present. Kulacki et al. (1981) is dedicated to the quantification of the temperature derivation process, and a flat rooftop is used to minimize possible interference with nearby structures. In both cases, presence of insulation, surface emissivity and captured moisture are main factors that affect the results of the analysis.

The majority of the surveys take pitched rooftops into consideration. Main factors that define thermal behavior of the pitched roof are pitch angle (expressed through view factor, as in Kulacki et al. (1981)), surface emissivity, insulation level and presence of ventilated attic. The importance of the latter is debated: Schott et al. (1982) states that ventilated attic might be ignored, if wind speeds are low. According to Brown et al. (1981), presence of ventilation drastically changes the thermal signature of the building, whatever wind conditions are. In any case, only a handful of papers (Birnie et al., 1984; Brown et al., 1981; Kulacki et al., 1981; Schott et al., 1982; Treado & Burch, 1981) mention convective heat loss (which must be analyzed to account for attic ventilation), and only Kulacki et al. (1981) and Schott et al. (1982) attempt to quantify it.

2.7.2 Walls

Two surveys (Anderson & Baker, 1987; Treado & Burch, 1981) mention possible relationships between the walls temperature and the heat "halo" around the building, usually seen on the aerial thermal imagery. This halo is a result of reflecting and re-emitting of thermal radiation by the ground surface. Treado and Burch, (1981) attempted to derive the temperature of the object using its halo, but no clear relationship was found. Taking a different point of view (quite literally), a study by Baraniak and Williams (1981) presents an example of ground-based thermal imaging survey that deals with the building's walls directly. Ability to capture oblique imagery of the building would add another dimension to the heat loss studies.

2.7.3 Pipelines

Anderson and Baker (1987), Birnie et al. (1984) and MacKay (1984) illustrate that aerial infrared imagery is convenient and cost-efficient when heat loss from buried pipelines is analyzed. As shown by MacKay (1984), pipelines locations must be known during the analysis part because of the vast range of surface types, which may completely mask the thermal trace. Even though pipelines insulation leaks are very easy to spot, they are quite difficult to quantify due to the complexity of the models involved. It is necessary to account for pipe burial depth, insulation level (which cannot be derived from remote sensing data) and surface emissivity.

Anderson and Baker (1987) and MacKay (1984) mention the presence of the workload on the system as an important factor. Studies of residential areas, such as Baraniak and Williams (1981) and Birnie et al. (1984), make emphasis on the patterns of

air conditioning usage, as well as the number of floors and the "distribution" of occupants within the building.

2.8 Summary

A list of requirements for a successful aerial survey emerged after the review of this literature had been completed. Quite demanding, it was not fully satisfied by any of the existing surveys. The list of requirements is presented:

- sensor with in-flight blackbody calibration
- ground temperature sampling
- ground emissivity sampling
- emissivity table for the region of interest
- ground meteorological survey
- heat radiation transmission models for objects of interest
- RTMs (existing or ad-hoc)
- intelligent questionnaires (for residential areas)
- infrastructure data (for industrial areas)

Thermal imagery, independent of its source, requires significant amount of processing. If done manually, it will jeopardize the effectiveness of the study. Geometrical and radiometrical correction of the images must be performed, ground control data must be collected and automated means of analysis must be found in order to fully employ the benefits of remote sensing approach.

For all the aerial surveys mentioned in this literature review data analysis is manual and error-prone. For residential areas (Anderson & Baker, 1987; Baraniak & Williams, 1981; Birnie et al., 1984), public attention, usage of intelligent questionnaires and data dissemination are highly important. Local knowledge of the building insulation parameters and occupants' behavior is an invaluable asset in the process of data analysis. For industrial areas (Anderson & Baker, 1987; MacKay, 1984), local knowledge of the facility engineers must be employed to maximize useful outcome from the thermal imagery.

CHAPTER 3

METHODOLOGY

3.1 Study Area

The proposed study area for this survey is the Campus of the University of Northern Iowa. Insufficient levels of heat insulation of dormitories, on-campus apartments, classrooms and laboratories may cause an increase of financial burden on UNI students and taxpayers. Therefore, such a study should be highly important for all campus inhabitants.

Despite its small area (about 2 km sq.), UNI Campus represents a wide variety of objects of interest, including flat rooftops, sloped rooftops, underground pipelines, heat exhausts and other infrastructure. This survey encounters a broad spectrum of surface materials, which has to be accounted for during the analysis part of the research.

The study area contains a high number of obstacles that would modify the local airflow. Therefore, variations in microclimate should be expected. Campus has a local meteorology station that can be used to assess changes in air temperature, humidity and pressure.

3.2 Data Collection

This project collects both aerial and ground level data.

3.2.1 Aerial Data Collection

Aerial data was collected by the private contractor, AITScan (a division of Stockton Infrared Thermographic Services, located in Randleman, North Carolina) on

April 04, 2007. The survey was performed between 11PM and 12AM to ensure maximum thermal contrast between the objects of interest (buildings, steam pipelines) and their surroundings (Anderson & Baker, 1987; Titman, 2001). AITScan used the thermal infrared camera "Phoenix-Mid" manufactured by FLIR Systems. This camera has a resolution of 640 x 512 pixels with a FOV of 14.6°. With the average flying height of 600 m above the ground level, ground resolution is approximately 0.29 m for the whole dataset. This camera has a radiometric resolution of 14 bits and operates in the wavelength range of 3.0 - 5.0 μm, perceived as a single band. Cooling is provided by the on-board Stirling closed cycle cooler.

Imagery is provided by AITScan in two formats, JPEG and SAF (Standard Archive Format). The JPEG file format in not capable of storing original 14 bit data (maximum bit depth is 8 bit for the gray channel). SAF files, on the other hand, contain full 14 bit camera output (stored in 16 bit form for convenience), as well as camera calibration coefficients that are used to convert pixel values to temperature and radiance. The SAF file is, in essence, an archive, that stores time series of imagery in the single-file form. This survey produced 24 SAF files, corresponding to the 24 flight lines. With each flight line consisting of approximately 250 separate images, the resulting dataset contains about 6,000 rasters.

3.2.2 Ground Data Collection

In order to provide additional control over the results of the survey, ground-level temperature data was collected. A handheld infrared thermometer ("MT4 Minitemp" manufactured by RayTek) was used for temperature sampling. According to the

manufacturer, the accuracy of "±2%, or ±1.7°C, whichever is greater," can be achieved. Previous to taking any measurements, this thermometer was tested and calibrated in a laboratory setup, as illustrated by Figure 1.

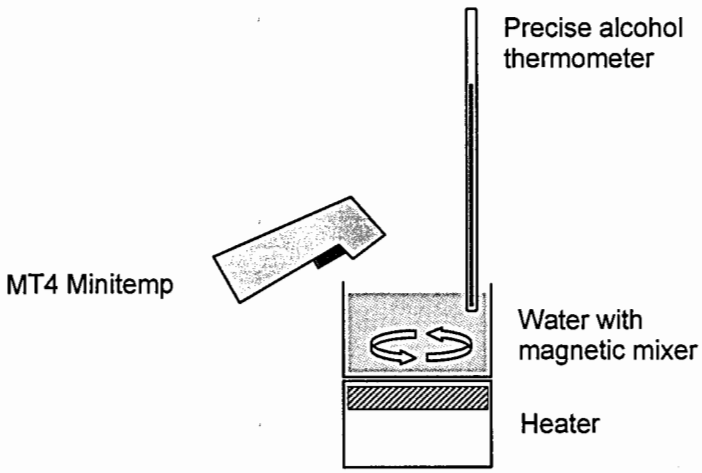

Figure 1. Infrared thermometer calibration.

A cup of cold water (around 1°C) was set up on a heater. A magnetic mixer at the bottom of the cup was constantly rotated by the magnetic field created by heater. The heater was turned on and as the temperature rose, simultaneous measurements were taken by the infrared and calibrated alcohol thermometer. Measurements were taken until the water reached 21°C. Then, the difference between two sets of temperatures was calculated. The differences were normally distributed with a mean of 0.4°C and standard deviation of 0.16. This test demonstrated that in the temperature range of 5°C to 20°C the accuracy was approximately ±0.3°C.

Ground control dataset consisted of 45 temperature measurements taken around the campus. 30 of 45 points were taken on concrete surfaces, the rest of them fall randomly between grass, bricks and metal. GPS unit with differential correction was used to record the location of the samples. In addition to these samples, two reference targets - two sheets of plywood, 2.5 by 1.2 m, covered in black matte paint - were set up two hours before the start of the survey, approximately 1 m above the ground level, as far from expected sources of thermal pollution as possible (Birnie et al., 1984). The immediate surroundings of both reference targets are shown on the Figure 2.

Figure 2. Location of the reference targets.

The first sheet was set up in the parking lot to the west of the Schindler Education Center (the lot was empty at the time of the survey), the second one was installed in the middle of the grass field to the south of the Lawther Hall.

These reference targets were later used in three different ways. First, both targets were used together with other ground samples to verify the pixel to radiance conversion model. In case the GPS positioning error would be too high to reliably identify the ground samples on the thermal imagery, two plywood targets would be a fall-back option to get at least some data for the model verification. Based on the proposed spatial resolution of 0.29 m, the size of the targets used would be enough for an accurate visual location. Second, the plywood targets were used to investigate the change of the temperature of the exposed objects overnight. The sampling period was selected to match the data collection interval of the on-campus meteorology station. Third, given the absence of any heat sources within or in the vicinity of these reference targets, they would enter the state of the thermal balance with their surroundings. The temperature of these two objects would then serve as a reference point in the assessment of the temperatures of the rooftops on campus.

Data from the on-campus automatic meteorology station located on the rooftop of the Latham Hall were collected every 30 minutes and contained temperature, pressure, and relative humidity values. Data on wind direction and speed were obtained from the nearby (6 km) meteorology station in Waterloo, Iowa. Throughout the night, the ambient air temperature stayed close to -6 °C, with humidity of 79%. Wind direction and speed were stable for the whole time of the survey (330°, 8 m/s). Except for the wind speed,

meteorological conditions were favorable for the thermal infrared survey – clear sky, low ambient temperatures and absence of precipitation all benefit thermal contrast (Anderson & Baker, 1987; Birnie et al., 1984).

3.2.3 GIS Data Collection

Thermal imagery requires significant amount of processing. Automated means of analysis must be found in order to fully employ the benefits of remote sensing approach. Using GPS coordinates as a spatial reference, ground control samples were transformed into a shapefile. Next, the raster extraction tool from the ESRI ArcGIS toolbox was used to extract matching pairs of aerial and ground measurements. Another shapefile with on-campus buildings was prepared by digitizing a high-resolution raster image in ArcMap. This shapefile was used to analyze raster data separately for every building. Finally, a shapefile with the structure of the UNI steam pipeline network was provided by the facility services department. This shapefile was used to locate the segments of the steam network that were in any way obscured on the thermal image.

3.3 Georeferencing and Mosaicing

As was mentioned before, aerial data was provided in the form of SAF files, which is an archive that stores a time series of images in the single-file form. In order to access individual raster images, another format had to be used. Portable Network Graphics format was chosen because it supports 16-bit grayscale data as well as lossless compression. An open-source software library, libpng (n.d.), was used to create PNG rasters. Raw data was extracted from the SAF files with a small application written by the author of this paper in compliance with SAF specifications.

Before georeferencing and mosaicing, a histogram of the pixel values distribution was created (Figure 3).

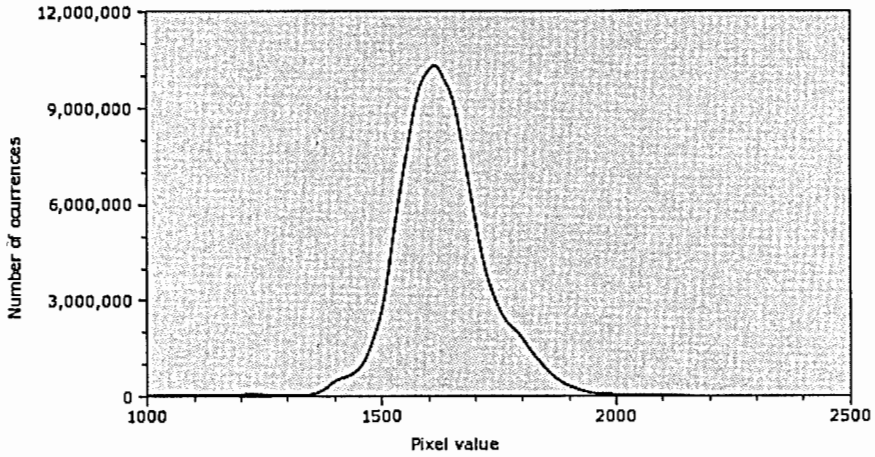

Figure 3. Pixel values distribution.

From the histogram, it is clear that the majority of pixels belong to the range of values between 1,300 and 2,100, which corresponds to less than 5% of the 16-bit range used by the camera. In order to improve visual contrast, the image histogram was stretched accordingly, using 850 and 2,835 as boundaries. Figure 4 is an example of an image before and after the histogram stretch. These boundary values were selected according to the Chebyshev's Inequality which guarantees that, independent of the exact form of the data distribution, no more than $\frac{1}{k^2}$ of the values are more than k standard

deviations away from the mean. For the selected boundaries, Chebyshev's Inequality guarantees that 99% of the dataset are within the range specified.

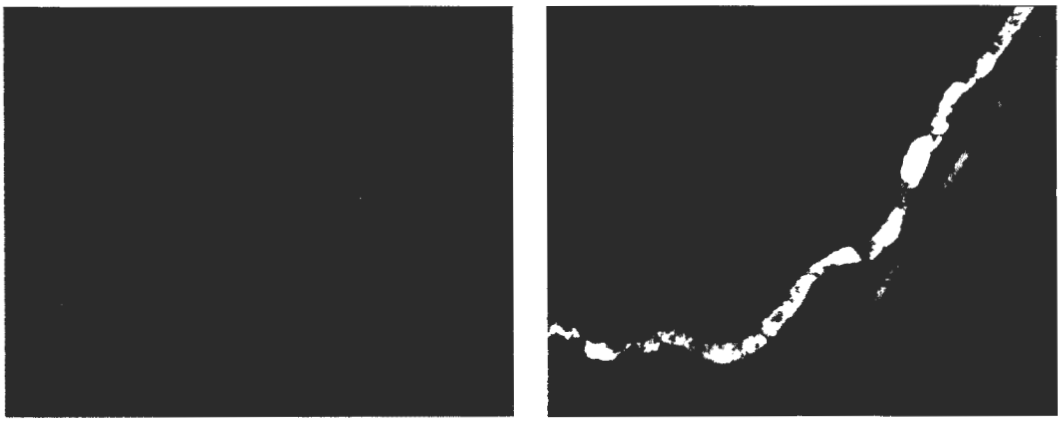

Figure 4. An image before (left) and after (right) the histogram stretch.

After stretching the histogram, raster images were mosaiced manually in the ERDAS Imagine software using existing high-resolution airborne imagery of the UNI Campus as a reference. RMSE for the resulting model were normally distributed with mean of 1.94 pixels and standard deviation of 0.69.

3.4 Pixel to Radiance Conversion

There are two common ways to convert pixel values to temperature. The first approach, utilized by Kulacki et al. (1981), MacKay (1984) and Tanis and Sampson (1977) is to convert pixel values into temperature directly by means of a regression model.

The second approach is to convert pixel values to radiance, then use the radiance values as an input to the Planck's formula, as was done by Schott and Wilkinson (1981) and Schott et al. (1982). This approach is a combination of a pixel-to-radiance regression model and the Planck's formula.

In this study, the second approach was used, because it provides additional control over the level of emissivity of the objects of interest. It was initially planned to convert pixel values into radiance by using conversion polynomials of the form

$$R = \sum_{i=0}^{n} c_i \cdot p^i$$

where c_i are calibration coefficients and p is the pixel value. Calibration data for the sensor was gathered on board the plane using a black body as a reference, as was done by Brown et al. (1981), MacKay (1984) and Tanis and Sampson (1977). However, the resulting polynomials produced erroneous temperatures that did not correspond to the ground truth. Instead, the dataset that was supposed to act as ground truth was used to create the regression model for the pixel to radiance conversion.

The regression model was built in two steps. First, using Planck's Law:

$$R(\lambda,T) = \frac{B}{\lambda^5 \cdot \left(e^{\frac{A}{\lambda T}} - 1 \right)}$$

where $A = \frac{hc}{k}$, $B = 2hc^2$, h is the Planck constant, k is the Boltzmann constant and c is the speed of light, the radiance of the ground samples was calculated as a function of their temperature. Only samples with well-known emissivity levels (concrete pavements) were used in this process. In the second step, ESRI ArcGIS was used to extract pixel values from the mosaiced thermal image at the locations of the ground samples. Then a linear regression model was built with the pixel values and radiance as variables.

The resulting model has a coefficient of determination (R^2) of approximately 0.78. However, the model is only reliably defined for the range of pixel values between the coldest and the hottest object sampled (approximately -12°C and 2°C). Using the model produced in the steps above, as well as the inverted version of the Planck's Law,

$$R(p) = 3.58838 \cdot 10^{-4} \cdot p - 0.290$$

pixel values were converted into temperatures. The level of emissivity was fixed at 0.95, which is the emissivity of concrete, according to the ASTER Spectral Library.

3.5 Thermal and Visual Data Overlay

Thermal imagery helps locate the hot spots, but it does not always reveal their source. Most of the times it is possible to make an educated guess about the source of the heat. However, to simplify the process of image interpretation, an attempt was made to combine visual and thermal infrared data using the overlay technique. Thermal imagery was corrected for the perspective distortion using high-resolution airborne imagery as a

reference, then ArcGIS was used to produce the overlay rasters. An example of the thermal data overlay is presented in the Figure 5 (the building shown is the Towers Center).

Figure 5. Thermal data overlay, Towers Center.

3.6 Analysis of Temperature Change Over Time

As it was mentioned before, the survey was performed between 11PM and 12AM and was, therefore, one hour long. An attempt was made to estimate the change of the temperature over the time of the survey to prove that the temperature maps are temporally consistent.

A number of images from the infrared imagery dataset (flight lines 16 and 24) were found to be identical in the spatial sense, but set 50 minutes apart in the temporal dimension. Seven pairs of spatially-overlapping images (shown on the Figure 6) were extracted from their flight lines and compared in ArcGIS. A local power plant can be seen between the pairs 5 and 6. Changes in temperature between the images in each pair were then calculated and stored both as raster files for visual inspection and as text files for statistical analysis. The process of temperature change estimation is illustrated by the Figure 7 (pair of images #3, a parking lot to the west of the WRC complex, is shown). Red areas of the raster image correspond to the areas of maximum change, whereas blue areas indicate little or no change at all. Temperature changes for each pair of images were tested for normality and plotted as a histogram. The results produced by this method were compared to the time series data obtained from the meteorological station and the reference targets.

3.7 Model Validation

Some of the ground samples were left for the model validation process. Once again, ArcGIS was used to extract temperature values at the locations of the validation samples. Temperature estimates produced by the model were then compared with the ground measurements.

Figure 6. Locations of the overlapping image pairs.

Figure 7. Temperature change estimation.

CHAPTER 4

RESULTS AND DISCUSSION

This chapter presents the results of the thermal infrared survey of the University of Northern Iowa campus. First, a general description of the thermal imagery is given in the section 4.1 ("Thermal Map of the UNI Campus"). An in-depth discussion of the hot spots detected is presented in the sections 4.2 "On-campus Buildings" and 4.3 "Steam Pipelines". An attempt at GIS-based data analysis is discussed in section 4.4 "Automated Analysis". Finally, the accuracy and temporal consistency of the models and data produced are discussed in sections 4.5 ("Analysis of Temperature Changes Over Time") and 4.6 ("Model Validation").

4.1 Thermal Map of the UNI Campus

Figure 8 shows the surface temperature variation map of the campus. This map clearly depicts the general distribution of temperatures on the campus. Areas covered in vegetation tended to exhibit lower temperatures, whereas man-made pavements with high thermal inertia were relatively warm. Overall, places with lower height, tall vegetation or clusters of buildings tended to be warmer than high, open grounds, because they are less exposed to the cooling effect of the night sky. An area of elevated temperature, a "heat island", is visible in the central part of the campus. Another easily spotted object is a small local stream (Figure 8, bottom right corner) - due to high thermal capacity of water, its warm stream is clearly outlined on the cool background. This study focused on two main objects of interest, on-campus buildings and underground steam pipelines.

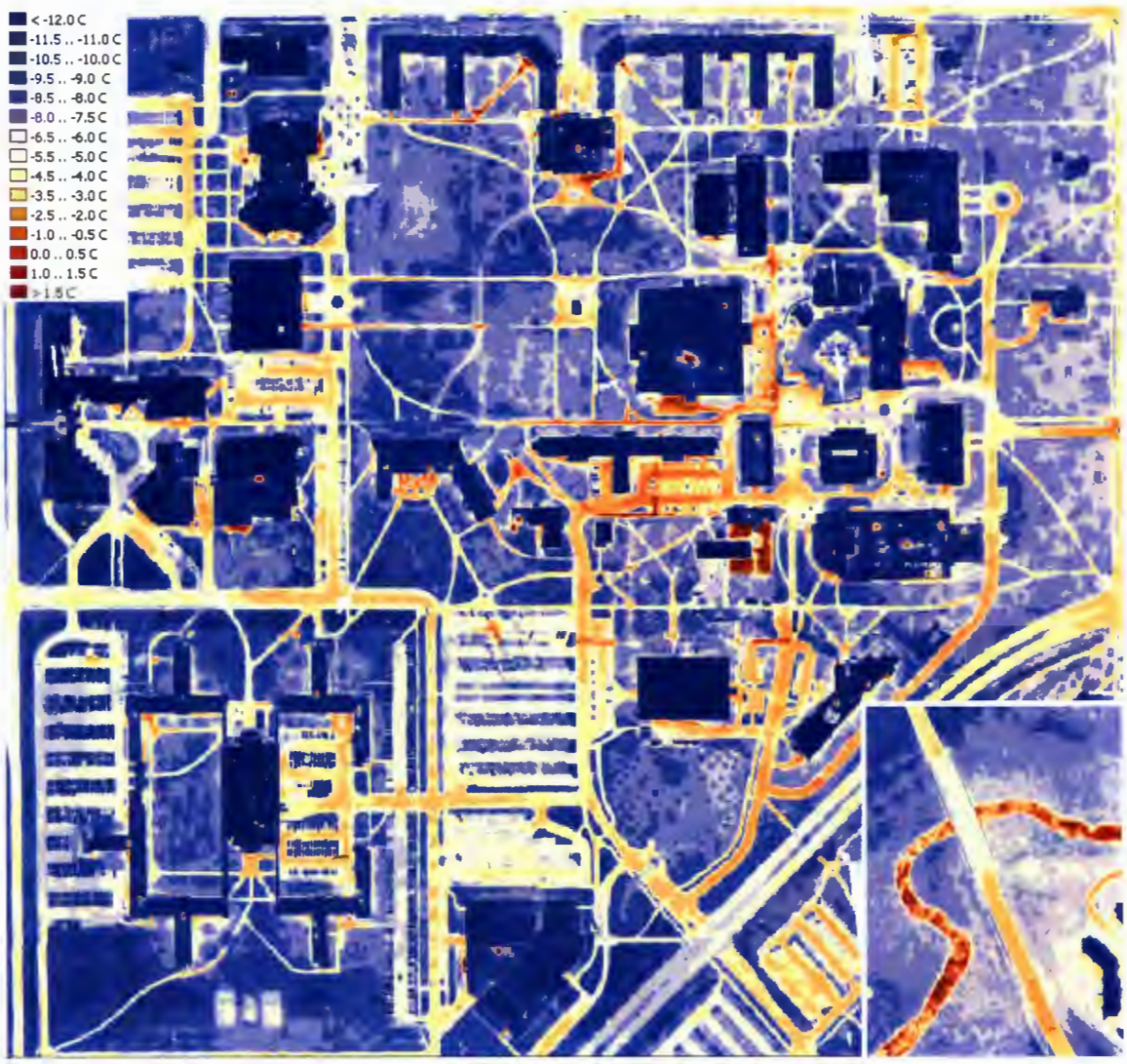

Figure 8. Thermal map of the campus.

4.2 On-campus Buildings

In general, rooftops of the buildings on campus are in good condition with no major leaks visible (a map of buildings on campus is presented in Appendix A, Figure A1). Some buildings have roof temperatures elevated above the average level, as well as

smaller issues. For example, Maucker Union (Figure 9) has the warmest rooftop of all the buildings on campus. Latham Hall (Figure 10) has an irregular hotspot on its rooftop that might be attributed to the elevated levels of moisture (Schott & Wilkinson, 1981). McCollum Science Hall (Figure 11) contains a number of chemistry labs that are well ventilated, which might explain the high number of hot spots found on its rooftop.

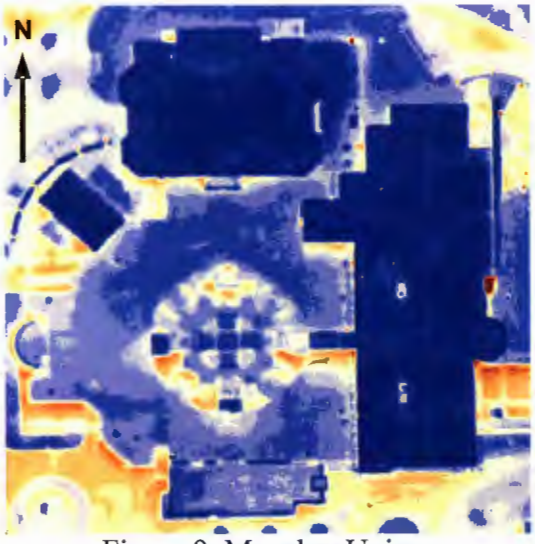

Figure 9. Maucker Union.

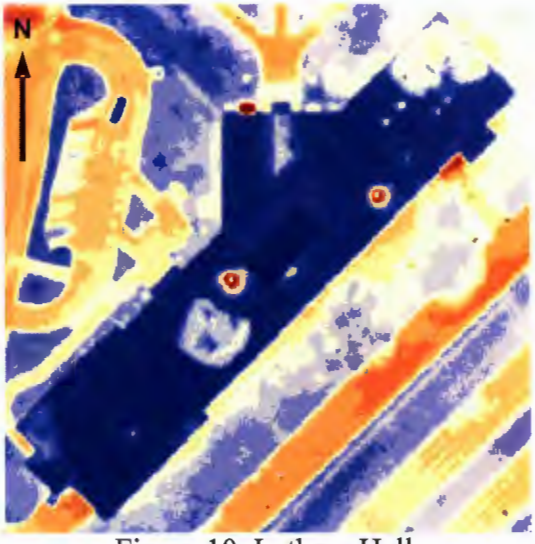

Figure 10. Latham Hall.

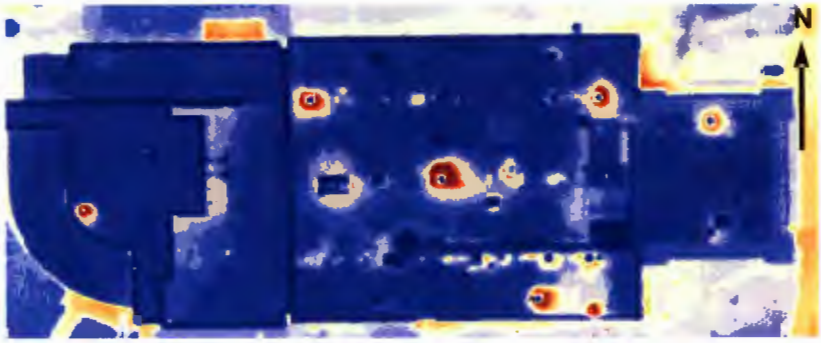

Figure 11. McColum Science Hall.

As the exact cause of the hot spot if often unclear, a digital combination of visual and thermal infrared data – thermal imagery overlay – was used to avoid making educated guesses about the source of the heat. An example of the thermal data overlay is presented in the Figure 12 (the building shown is the Rod Library). The main hot spot in the middle of the rooftop is clearly attributed to the ventilation exhausts. Four other small spots are also easily identified as smaller vents.

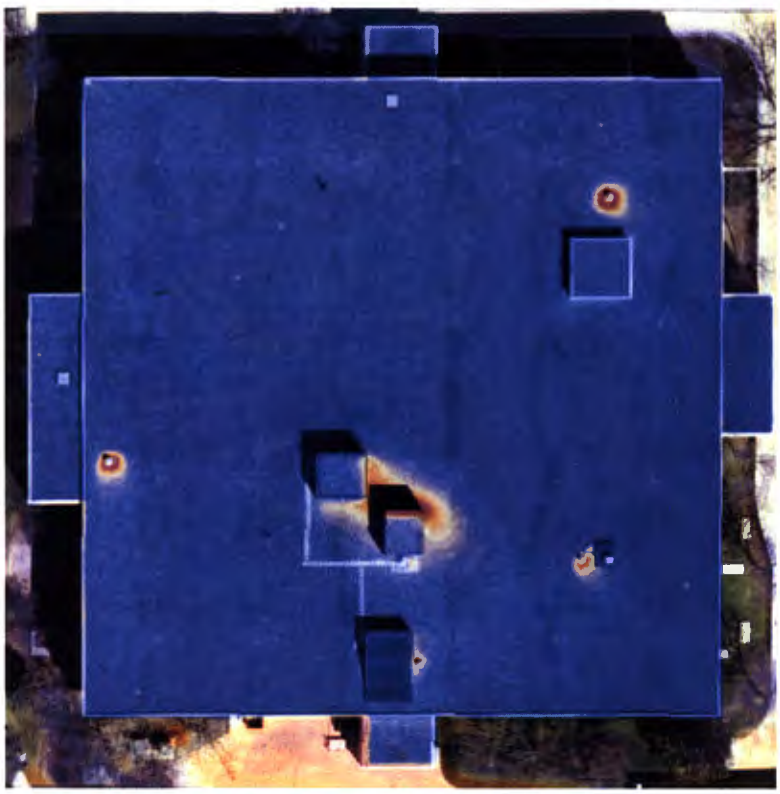

Figure 12. Thermal data overlay, Rod Library.

Another good example is the image of the McCollum Science Hall, presented in the Figure 13. Compared to the Figure 11, this image now clearly shows that the majority of thermal anomalies are caused by the ventilation exhausts. The fact that this building had the most hotspots of all the other buildings on campus is, as suspected, explained by the number of ventilated labs that McCollum Science Hall contains. Direct interpretation of the thermal image was, in this case, somewhat cumbersome.

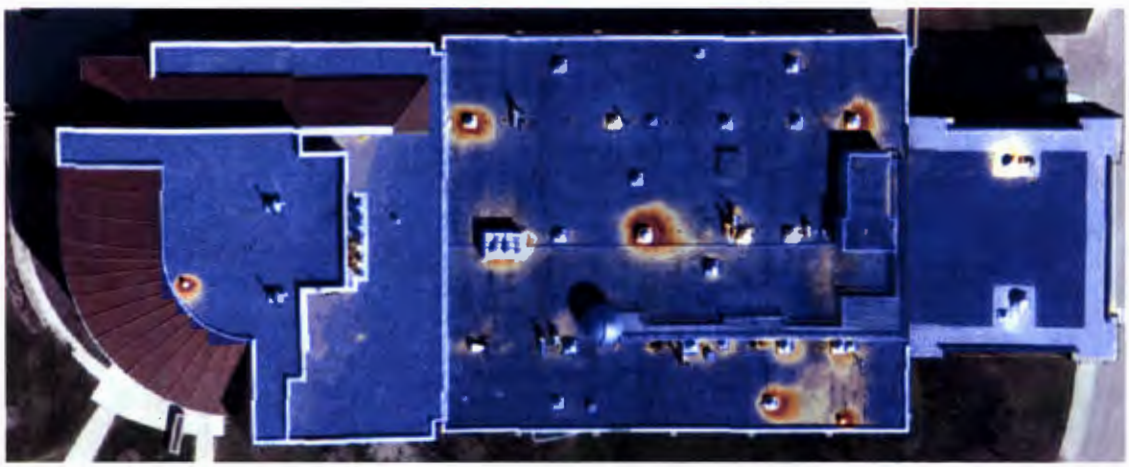

Figure 13. Thermal data overlay, McCollum Science Hall.

For most of the on-campus buildings, vents are operating in particular modes that correspond to the time of the day and to the kind of the load being served. For example, bathrooms in the dormitories are ventilated throughout the whole day because of the heavy load they receive all the time. Swimming pool areas are constantly ventilated as well to prevent accumulation of chlorine. The majority of the vents, however, were

turned off for the time when this survey took place. Redeker Hall (shown in the Figure 14) illustrates the principle of the nighttime operation mode.

Figure 14. Thermal data overlay, Redeker Hall.

This building contains a number of kitchens and eateries for the neighboring dorms and, as a consequence, its rooftop is decorated with ventilation exhausts of all possible types. Most of them, however, are offline with only trace amounts of heat

escaping the vents. The only exception - a large ventilation exhaust, located in the southwestern corner of the building, is serving the computer lab located in the Redeker Hall, and has to work throughout the night.

Another interesting aspect of the on-campus buildings is that some of the rooftops are ballasted (have a layer of gravel or broken stone laid on top of them). It is an older technology, which is nowadays only used to enhance the acoustic qualities of the buildings, such as the Gallagher-Bluedorn Performing Arts Center. Uneven levels of ballast can cause water to pool on the rooftops, which, with time, deteriorates insulation. A number of spots were located where the pooling of water might be taking place. Field inspection proved that water pooling was indeed happening, both on ballasted and non-ballasted rooftops.

An example of moisture accumulating on top of the building is presented in the Figure 15 (the building shown is the Latham Hall). Two small hotspots are easily noticed that correspond to ventilation exhausts. Two other, less pronounced and more spatially spread hotspots can also be found which are not attributed to any of the infrastructure present on the rooftop. These hotspots are the thermal image of the standing water, initially suspected by their irregular shape and lack of obvious source and later confirmed by the visual inspection.

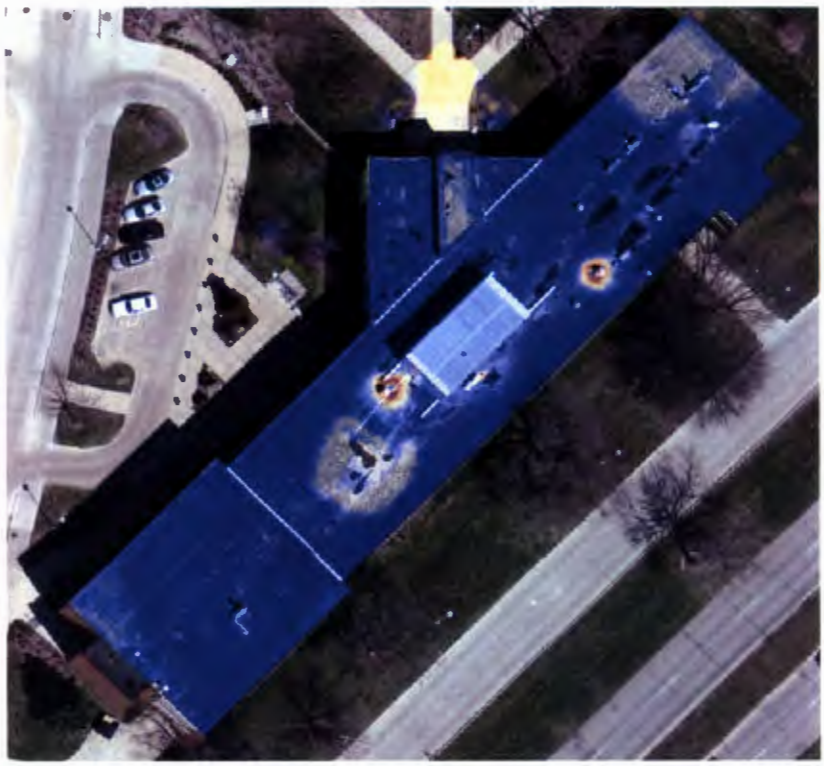

Figure 15. Thermal data overlay, Latham Hall.

Another example of this problem is the rooftop of the Rider Hall, shown in the Figure 16. This building has a ballasted rooftop - as mentioned earlier, it was built by an older technology. Rider Hall four ventilation exhausts on its rooftop that are clearly marked by the hotspots. The eastern wing of the building also has two less pronounced anomalies in its northern and southern parts. Once again, water pooling was suspected, which was confirmed by the visual inspection. In this case, water pooling was caused by uneven levels of ballast, which slowed the drainage of the rainwater and dew. As it was mentioned before, this eventually leads to insulation deterioration.

Figure 16. Thermal data overlay, Rider Hall.

Finally, some of the buildings on campus have a slanted wooden rooftop. Lang Hall (that, as a matter of fact, has one of the oldest roofs on campus) belongs to this category. The attic floors of such buildings are normally insulated with blocks of foam (in case of the Lang Hall, insulation was retrofitted), but the slanted roof itself does not have any insulation whatsoever. Also, this attic is used to house some of the air conditioning equipment that Lang Hall is making use of. This equipment is raising the temperature in the attic significantly and, to prevent condensation in wintertime, the attic

is artificially ventilated. Older dorms have problems similar to the Lang Hall. The attic floors in the Bartlett and Lawther Hall either have retrofitted insulation, or don't have any. Numerous infrastructure upgrades required artificial ventilation to be set up in their attics to prevent condensation. Presence of heat sources above the main layer of insulation combined with the forced ventilation causes the entire surfaces of the rooftops of these buildings to stand out in the thermal imagery.

When subtle variations of temperature were of interest, it was useful to improve the contrast of the imagery on the building-by-building basis. Instead of using the temperature distribution of the entire campus in the display scale, separate images with different scales were created for the use of Facilities Planning department. Such imagery makes less pronounced effects, such as water pooling, stand out.

The raster products mentioned above (thermal overlay and high-contrast imagery) were found to improve the data readability greatly. These products, combined with the help of the Facilities Planning Dept, allowed deciphering most of the thermal anomalies previously found in the on-campus buildings.

For all buildings on campus, a so-called halo effect is present. Two surveys (Anderson & Baker, 1987; Treado & Burch, 1981) mention possible relationships between the temperature of the walls and the halo intensity. This effect is attributed to the reflection and re-emission of thermal radiation by the ground surface. Treado and Burch (1981) attempted to derive the temperature of the object using its halo, but no clear relationship was found. Nonetheless, this effect serves the purpose of illustrating the wind-sheltering effect (Treado & Burch, 1981) of the on-campus buildings. The direction

and the speed of the wind remained steady throughout the night (330°, 8 m/s). This contributes to the areas to the south of the structures being warmer than their northern counterparts.

As it was mentioned before, the halo effect is poorly suited for the analysis of wall temperatures. The study by Baraniak and Williams (1981) is an example of a ground-based thermal imaging survey that deals with the building's walls directly. Their study demonstrated that a number of significant temperature anomalies could be found by examining the structures from the side view. Because of the sharp turns the plane was performing at the end of each flight line, a number of oblique images of the buildings in the vicinity of the campus were produced. One of the best examples is present in the Figure 17. The building shown is Cedar Falls High School, located about 1 km to the north of the campus. The high visual contrast between the rooftop and the walls is obvious.

Although it is tempting to associate high visual contrast in this image with high temperature contrast in real life, a number of factors should be included. First of all, the emissivity of the exposed surface is anisotropic in nature. This effect is not pronounced in the nadir imagery, but is important as the angle of view deviates from nadir by more than 60 degrees (Cuenca & Sobrino, 2004). Second, no ground control samples are available for that particular location. It is, therefore, not possible to verify the remote sensing data for this area. Finally, only one side of the building was exposed to the camera and it is not possible to estimate the effect of the wind on the distribution of temperature across the surface of the building.

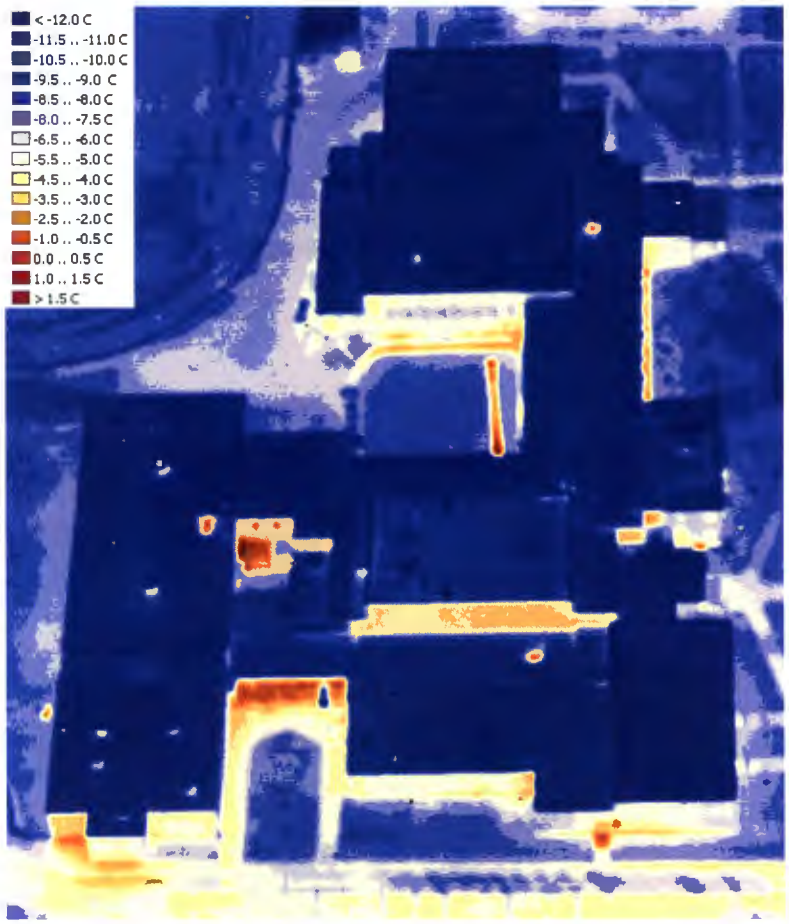

Figure 17. Oblique image of the Cedar Falls High School.

4.3 Steam Pipelines

Several papers (Anderson & Baker, 1987; Birnie et al., 1984; MacKay, 1984) illustrate that aerial infrared imagery is a convenient and cost-efficient tool when temperature anomalies in the steam pipelines network are being sought. As shown by MacKay (1984), pipeline locations must be known during the analysis because of the vast range of surface types, which may completely mask the thermal trace. Combined with the

shielding effect of the buildings, the heat coming from underground pipelines is the most possible explanation of the elevated temperatures in the central part of the campus. Compared to other objects of interest, steam pipelines stand out most vividly on the thermal imagery of the campus (Figure 18).

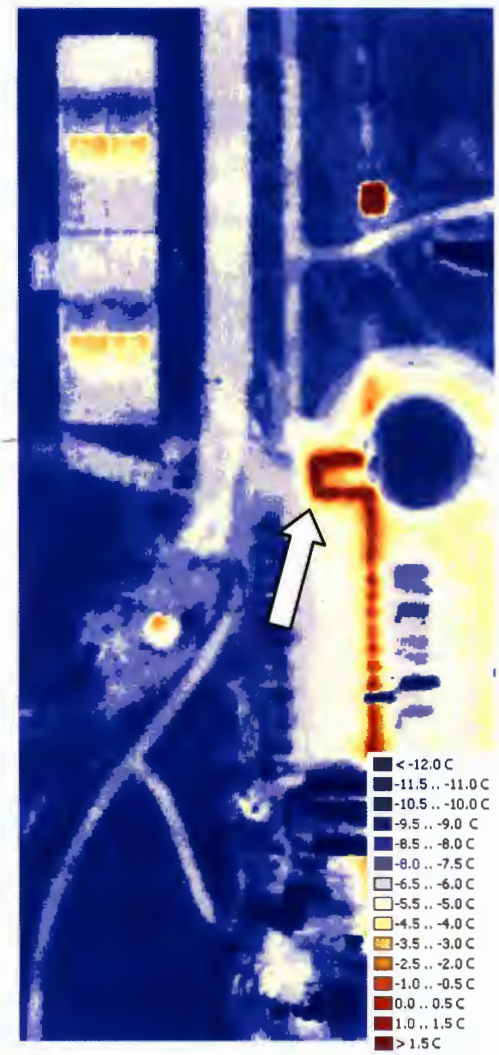

Figure 18. Steam pipelines.

There are two main types of steam pipelines on campus - directly buried pipelines and tunnels. Tunnels are more expensive to build, but are easier to maintain and provide longer life for the infrastructure they host. Tunnel-based pipelines require surface openings in the tunnel to allow for maintenance and ventilation. These correspond to some of the brightest hotspots, even though they are, technically, not a problem on their own. Some of the tunnels (and the piping they contain) is rather old, and becomes particularly visible on the thermal map. An example can be found to the south of the Baker Hall.

Directly buried pipelines are cheaper, but are nearly impossible to maintain. They require that vaults with steam traps are provided at regular intervals so that condensed water could be removed from the pipeline. These vaults are not insulated and are easily located on the thermal map as well. The most visible pipelines are of the directly buried type, such as the one shown earlier in the Figure 18. As Facilities Planning helped find out, this type of pipelines is prone to water infiltrating its outer layer of insulation, which further contributes to the amount of heat leaking from it. Directly buried pipelines on campus are currently being replaces by the tunnel based ones.

4.4 Automated Analysis

One of the issues not addressed in many papers is automated analysis of the imagery. As was mentioned in the "Methodology" chapter, a shapefile with vector representation of on-campus buildings was created. Using this shapefile and the extraction tool from the ESRI ArcGIS Toolbox, separate imagery datasets for each of the buildings were created. Pixel values from each dataset were extracted and could then be

used for any form of statistical analysis (in this case, something as simple as histogram plots). Histogram plots for the buildings on campus are presented in Appendix B, Figure B1. A number of examples are show in Figure 19 (polygons from the shapefile can be seen as the red outline). Histogram peaks define the most frequent pixel values (or temperatures, for that matter).

These histograms were used to compare the average temperatures of the buildings to two points of reference: the temperature of the ambient air and the temperature of the reference targets, described earlier in the "Methodology." It was found that the only objects with temperature higher than that of the ambient air were ventilation relieves and pools of accumulated moisture. This leads to conclusion that at the time of the survey, no convective heat loss was taking place from the rooftops of the buildings on campus. As to the reference targets, it was found that all of the dorms, as well as a number of non-residential halls, were slightly warmer than the expected -12.2°C.

As it was shown, GIS integration allows for automated numerical analysis of objects of interest. For the UNI Campus the benefits of automation are not so obvious, however, because of the low number of buildings. For surveys of large residential areas the importance of automation is significant.

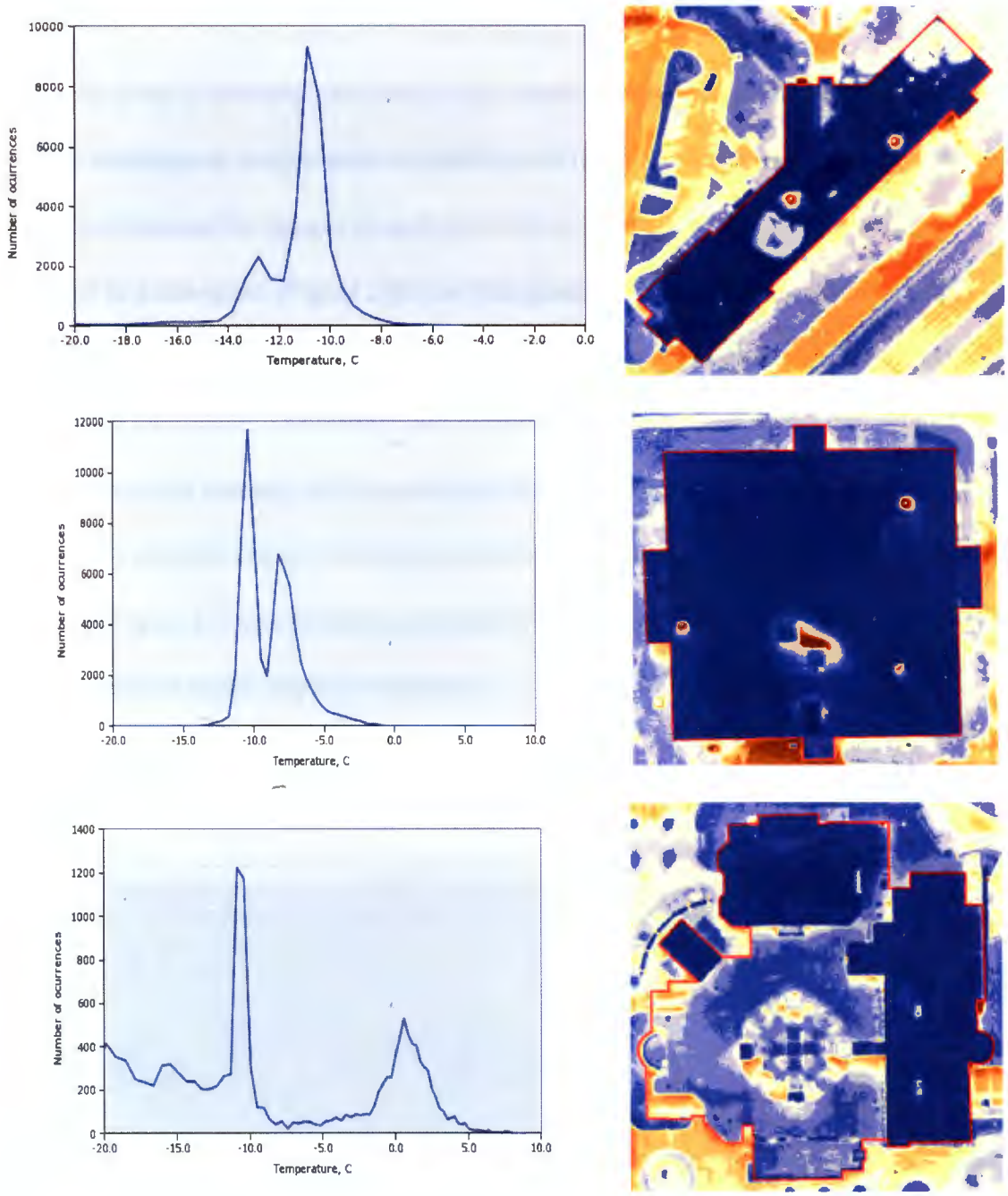

Figure 19. Temperature histograms of the individual buildings.

4.5 Analysis of Temperature Changes Over Time

As it was previously mentioned in the Methodology section, seven pairs of spatially overlapping images were overlaid in ArcGIS. Pixel-by-pixel temperature differences between the images in each pair were calculated and the results were presented as a histogram (Figure 20). The histogram clearly shows that for most of the images pairs 1 to 5 (referred to as "samples" farther on) a slight decline in the average temperature took place. The average temperature shift was estimated at 1.1°C, which is below the level of accuracy of the tools used for ground data collection (±1.7°C, as specified by manufacturer). A closer examination of the temperature difference rasters (shown in Figure 21) also revealed a number of cooling patterns that different types of materials exhibit under varying conditions.

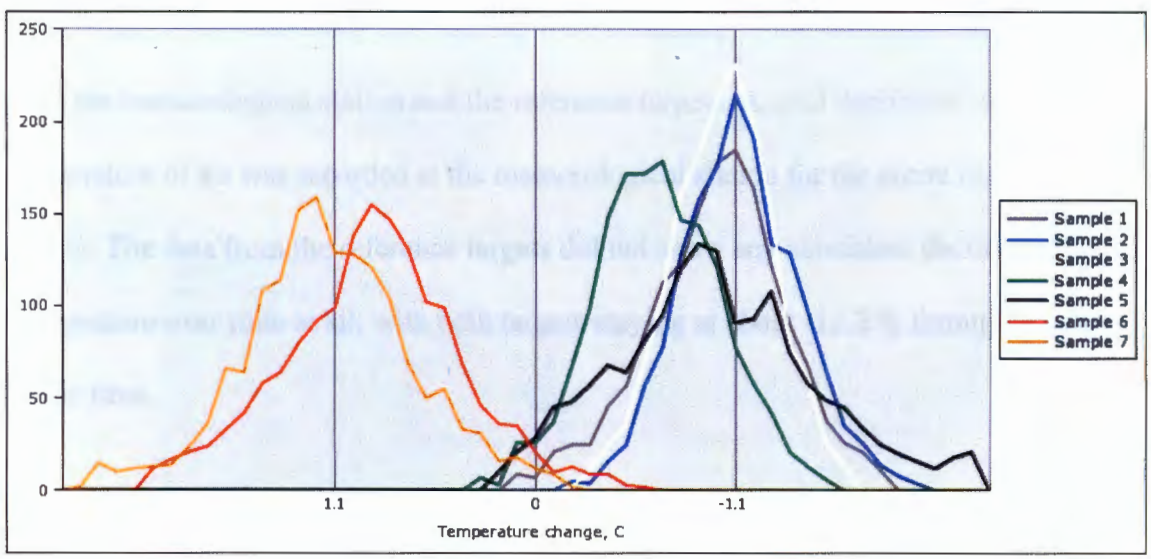

Figure 20. Histogram of the changes in temperature over time.

First, objects that had their temperature above the average level tend to cool faster. This is illustrated by the man-made materials with high thermal inertia (concrete pavements, parking lots, roads) showing up as red in the Figure 21. As it was mentioned before, red areas of the raster image correspond to the areas of maximum change, whereas blue areas indicate little or no change at all. Second, open and elevated areas that are more exposed to the night sky tend to cool off faster as well. This is illustrated by the presence of the slight gradient towards elevated areas in the temperature difference rasters. Third, proximity to objects that act as a heat source, such as the Wellness Recreation Center, tends to slow down the heat exchange, which shows up as another slight gradient. Given that the average change in temperature over the time of the survey did not exceed the accuracy of the tools used to perform it, as well as the apparently complex and location-specific nature of this phenomenon, no further investigations were performed.

The results shown by this method were compared to the time series data obtained from the meteorological station and the reference targets. A total decline of -0.6°C in the temperature of air was recorded at the meteorological station for the entire time of the survey. The data from the reference targets did not show any consistent decline in the temperature over time at all, with both targets staying at about -12.2°C throughout the whole time.

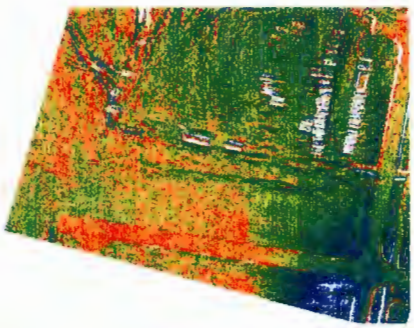

Sample #1

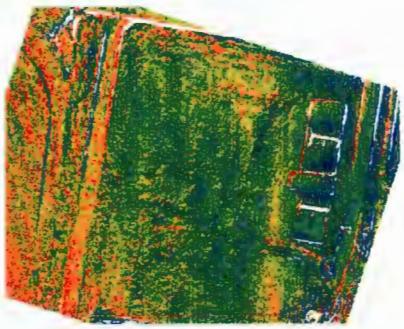

Sample #2

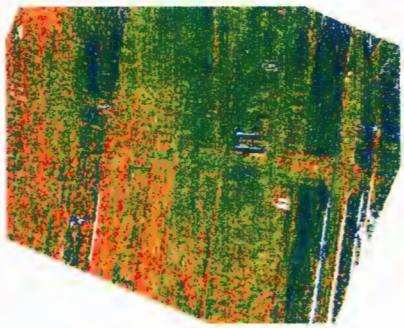

Sample #3

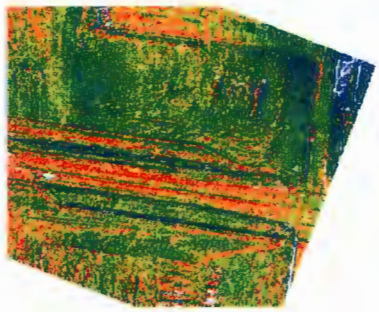

Sample #4

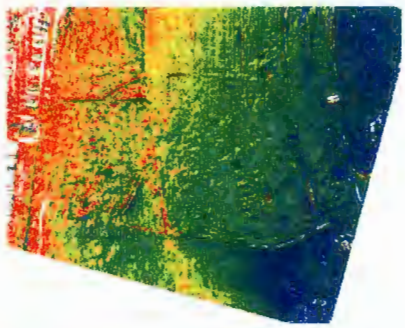

Sample #5

Sample #6

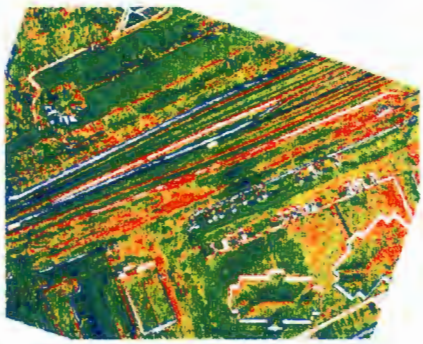

Sample №7

Figure 21. Changes in temperature over time.

It is interesting to note that samples 6 and 7 exhibit a completely opposite behavior when compared to the rest – their average temperature has actually raised by 1.1°C over the time of the survey. This peculiar behavior might be explained by the fact that these two sample areas are located directly to the south of the local power plant. Given the stable wind present at the time of the survey as well as the almost straight (330°) north-to-south direction of the wind, hot exhaust from the power plant might have changed the microclimate at the samples 6 and 7. Once again, the temperature change is below the accuracy of the surveying tools, and this example only serves to illustrate the complex interactions that exist on the microclimate level.

4.6 Model Validation

Temperature estimates produced by the model were compared with the ground measurements. The results of the validation are presented in Table 1. The mean temperature error is -0.25°C, standard deviation is 0.58°C. This makes the model accurate to within ±1.2°C.

Table 1. Error estimation.

Model temp., °C	Ground temp., °C	Error, °C
-8.1	-8.1	0.00
-5.2	-5.0	-0.17
-8.1	-7.8	-0.28
-6.9	-6.7	-0.28
-8.1	-8.9	0.78
-5.8	-5.0	-0.78
-4.9	-3.9	-1.06

Thermal infrared imagery collected in this survey has a radiometric resolution of 14 bits, which corresponds to the temperature resolution of 0.024°C. Such level of precision may seem unreasonably high compared to the average accuracy of the model. It is, however, important to understand that thermal imagery in this case is characterized by its relative accuracy. This means that 0.024°C is the smallest difference in temperatures that will be detected. Any errors in the original model would shift the temperatures of all the objects of interest by exactly the same value, retaining the temperature resolution of the imagery.

CHAPTER 5

CONCLUSIONS

In this chapter, the conclusions of this study are presented. Despite the fact that this work is generally considered a success, a number of important recommendations for similar studies are mentioned, along with the limitations of this work and possible directions for future research.

5.1 Conclusions

The main goal of this study was to produce and analyze a heat loss map of the University of the Northern Iowa campus using thermal infrared remote sensing data. This broad task was divided into three separate objectives, and the conclusions are presented in the similar manner.

The first objective was to produce high-quality thermal infrared imagery for the territory of the campus. Aerial data with the spatial resolution of 0.29m and radiometric resolution of 14 bit was collected, with the average spatial accuracy of 1.94 pixels. A model for the pixel to radiance and temperature conversion was developed with its parameters estimated with an R^2 of 0.78. Temperature imagery was shown to be consistent over the time of the survey and accurate to within 1.2°C. The resulting temperature maps are ready for further analysis and exist as a separate, high quality remote-sensing product. The first objective is, therefore, considered completed. A number of limitations and weaknesses in the data collected and of the methods used are outlined in the "Limitations" section of this chapter.

The second objective was to locate and explain the hot spots by analyzing the thermal infrared imagery obtained in the first step. Buildings and pipelines shown on the temperature map of the campus were the main object of interest in the analysis. Knowledge of the engineers from the Facilities Planning department was used to reliably identify the causes of all the thermal anomalies ("hot spots") detected.

Overall, infrastructure on campus is in good condition. Underground steam pipelines were found to create the biggest number of temperature anomalies. Despite the fact that some of the hot spots were false positives (such as the steam traps and maintenance vaults, which normally exhaust a large amount of heat), most of them were directly linked to the damage of insulation either by the infiltrating water or simply by age.

A heat island in the central part of the campus was detected, which was later explained by the unique combination of old tunnel-based pipelines, large quantities of concrete surfaces and dense construction. Old pipelines with deteriorated insulation produce heat and the concrete surfaces serve as a heat accumulator, while the cold night sky gets partially obscured by the nearby buildings.

Building-by-building hot spots analyses were performed using the products of the thermal data overlay. Ventilation exhausts and pools of accumulated moisture were found to be the main source of the hotspots. Some of the buildings had a surprisingly high amount of vents operating in the nighttime, which would be further investigated by the Facilities Planning department. Elevated temperatures of the rooftops of Lang, Bartlett and Lawther halls were explained by the presence of heat-emitting equipment

along with the forced ventilation in their attics. The ballasted rooftop of Rider Hall and the rooftop of Latham Hall were found to accumulate moisture because of the inefficient drainage.

The average temperatures of the buildings were compared to two points of reference: the temperature of the ambient air and the temperature of the reference targets. It was found that at the time of the survey radiative heat transfer was the dominant form of the heat loss.

The combination of temperature imagery, thermal data overlay and local knowledge, provided by the Facilities Planning department, did explain all of the hot spots found on the temperature map of the campus. From the practical point of view, this makes the second objective of this study completed.

Finally, the third objective was to assess the benefits of using the superior equipment and technology. Spatial resolution of 0.29 m was sufficient for the analysis performed in this study, but further reduction in the resolution would mask the difference between such distinct causes of hot spots as ventilation exhaust, pooled water and insulation deficiencies. Radiometric resolution of 14 bit gives an estimated 0.02°C per pixel count (for the dataset used in this study), while most widely used dynamic range of 8 bits would only give 1.6°C per count. Radiometric resolution, therefore, defines the extent to which subtle temperature gradients, such as those produced by pooled water and insulation deficiencies, stand out on the background.

Modern image processing techniques, such as thermal data overlay and thermal images with individual levels of contrast were found very useful in the process of data

analysis and interpretation. Given the simplicity of these techniques, the perceived increase in the usability of the final product of this survey was remarkable. A small example of the GIS analysis was also shown. Despite the generally positive results, the scale of this study was too small to appreciate the benefits of the GIS automation.

It was concluded that high spatial and radiometric resolution of the data, modern image processing techniques and an attempt at GIS analysis all contributed to the success of this study.

5.2 Limitations

This study consisted of many separate steps, with each step being a compromise between getting this study perfect and getting it done. Although this project is considered a success, the list of possible improvements and limitations starts from the moment of data collection and follows the flow of this survey to its very end.

The observation conditions mentioned in the beginning of the paper – cold, dry and clear April night – played a critical part in the success of this survey. First of all, this ensured maximum thermal contrast between the objects of interest (buildings, steam pipelines) and their surroundings. Second, the combination of the low flying altitude and a cold atmosphere reduced the absorption and emission of the infrared energy by the column of air between the sensor and the objects of interest. Finally, atmospheric effects are assumed to be the same over time because of the short duration of the survey and stable meteorological conditions. This approach would not suffice for a survey with different observation conditions.

Another limitation is that no measurements of the emissivity values of the objects in question were performed. Facilities Planning department agreed to provide the samples of all building materials used on campus. However, none of the spectrometers that are currently available to the UNI operate in the required wavelength range. Generic material categories, such as "concrete" or "grass" were used to obtain the emissivity values from the ASTER Spectral Library, which would introduce a certain degree of error into the radiance to temperature conversion. Given that the selection of the emissivity level does influence the derived temperature values directly, this is an important consideration.

This study would significantly benefit from a more extensive ground control dataset. Provided that more resources were available, time series of the temperature samples for multiple locations on campus should have been collected. Reference targets with a range of pre-set temperatures and emissivity values would improve the quality of the models built in this project. Variations in the microclimate were almost impossible to account for, and an extensive network of meteorological stations would be required to model this aspect of thermal infrared survey.

A significant limitation of this study is absence of proper on-plane camera calibration. As it was mentioned before, temperature values, calculated according to the calibration polynomials that were supplied with the imagery did match the ground control data at all. Part of the ground control data was used to construct the pixel-to-radiance conversion model instead, which ultimately resulted in a smaller validation dataset. A higher number of ground temperature samples, as well as time series of temperature data, are normally collected when the on-plane camera calibration data is not present.

Another issue that originated from the sensor was that of histogram stretch. Radiometric resolution was decreased by this required measure, and a much better solution would be to perform the aerial data collection in two runs – first to adjust the sensitivity of the sensor and second to actually collect the data.

Finally, in this survey, the process of mosaic creation was performed manually. Even though a high degree of accuracy was achieved, a significant amount of time was spent in the process. Larger studies should either employ image orientation data recorded in-flight, or use more sophisticated photogrammetrical software to automate the process. None of these options were available in this study.

REFERENCES

Anderson, J.M., & Baker, D. (1987). The thermographic survey of central Scotland. *International Journal of Remote Sensing, 8* (5), 779-788.

Baraniak, D.W., & Williams, C.E. (1981). Mobile ground-based infrared heat loss survey of 25000 buildings in West Allis, Wisconsin. *Proceedings of SPIE - The International Society for Optical Engineering, 313*, 50-60.

Becker, F., & Li, Z.L. (1990). Temperature-independent spectral indices in thermal infrared bands. *Remote Sensing of Environment, 32*, 17-33.

Birnie, R.V., Rithie, F.S., Stove, G.C., & Adams, M.J. (1984). Thermal infrared survey of Aberdeen City: data processing, analysis and interpretation. *International Journal of Remote Sensing, 5*, 47-63.

Brown, R.J., Cihlar, J., & Teillet, P.M. (1981). Quantitative residential heat loss study. *Photogrammetric Engineering and Remote Sensing, 47* (9), 1327-1333.

Colcord, J.E., & Asce, M. (1978). Thermal infrared imagery use in urban energy surveys. *American Society of Civil Engineers, Transportation Engineering Journal, 104* (5), 637-651.

Cuenca, J., & Sobrino, J.A. (2004). Experimental measurements for studying angular and spectral variation of thermal infrared emissivity. *Applied Optics, 43* (23), 4598-4602.

Gillespie, A.R. (1985). Lithologic mapping of silicate rocks using TIMS. *Proceedings of the Thermal Infrared Multispectral Scanner (TIMS) Data User's Workshop* (pp. 29-44). Jet Propulsion Laboratory (JPL) Publication 86-38 (Jet Propulsion Laboratory, California Institute of Technology, Pasadena, CA).

Gillespie, A.R., Rokugawa, S., Matsunaga, T., Cothern, J.S., Hook, S.J., & Kahle, A.B. (1998). A temperature and emissivity separation algorithm for advanced spaceborne thermal eimssion and reflection radiometer (ASTER) images. *IEE Transactions on Geoscience and Remote Sensing, 36*, 1113-1126.

Gu, D., & Gillespie, R. (2000). A new approach to temperature and emissivity separation. *International Journal of Remote Sensing, 21* (10), 2172-2132.

Kealy, P.S., & Gabell, A.R. (1990). Estimation of emissivity and temperature using alpha coefficients. *Proceedings of second TIMS workshop* (pp. 11-15). Jet Propulsion Laboratory (JPL) Publication 90-95 (Jet Propulsion Laboratory, California Institute of Technology, Pasadena, CA).

Kidder, S.Q., & Vonder Haar, T.H. (1995). *Satellite Meteorology: an Introduction* (1st ed.). London: Academic Press.

Kulacki, F.A., Mintzer, O.W., & Winget, L.E. (1981). Remote sensing of building heat loss - a case stuffy for development of methodology. *Proceedings of SPIE - The International Society for Optical Engineering, 313*, 139-150.

Kumar, A., Minnet, P.J., Podesta, G., & Evans, R.H. (2003). Error characteristics of the atmospheric correction algorithms used in retrieval of sea surface temperatures from infrared satellite measurements: global and regional aspects. *Journal of the Atmospheric Sciences, 60* (3), 575-585.

Kumar, A., Minnet, P.J., Podesta, G., Evans, R.H., & Kilpatrick, K. (2000). Analysis of Pathfinder SST algorithm for global and regional conditions. *The Proceedings of the Indian Academy of Sciences: Earth and Planetary Sciences, 109* (4), 395-405.

libpng (n.d.). *Open source software library.* Retrieved October 24, 2008 from http://libpng.org/pub/png/libpng.html

MacKay, H.W. (1984). Airborne thermal infrared scanning for district heating maintenance programs. *Proceedings of the Annual Conference of the International District Heating Association, 75,* 534-537.

McMillin, L.M. (1975). Estimation of sea surface temperature from two infrared window measurements with different absorption. *Journal of Geophysical Research, 80,* 5113-5117.

Nowak, H. (1989). The sky temperature in net radiant heat loss calculations from low-sloped roofs. *Infrared Physics, 29*, 231-232.

Ottle, C., & Vidal-Madjar, D. (1992). Estimation of land surface temperature with NOAA9 data. *Remote Sensing of Environment, 40*, 27-41.

Prata, A.J. (1993). Land surface temperatures derived from the advanced very high resolution radiometer and the along-track scanning radiometer. Theory. *Journal of Geophysical Research, 98*, 16689-16702.

Schott, J.R., Biegel, J.D., & Wilkinson, E.P. (1982). Quantitative aerial survey of building heat loss. *Proceedings of SPIE - The International Society for Optical Engineering, 371*, 187-195.

Schott, J.R., & Wilkinson, E.P. (1981). Quantitative methods in aerial thermography. *Proceedings of SPIE - The International Society for Optical Engineering, 313*, 20-27.

Swinbank, W.C. (1963). Longwave radiation from clear skies. *Quarterly Journal of the Royal Meteorological Society, 89*, 339-348.

Tanis, F.J., & Sampson, R.E. (1977). Application of airborne infrared technology to monitor building heat loss. *Proceedings of the International Symposium on Remote Sensing of Environment, 2*, 1001-1013.

Titman, D.J. (2001). Applications of thermography in non-destructive testing of structures. *NDT and E International, 34* (2), 149-154.

Treado, S.J., & Burch, D.M. (1981). Field evaluation of aerial infrared surveys for residential applications. *Proceedings of SPIE - The International Society for Optical Engineering, 313*, 28-34.

Voogt, J.A., & Oke, T.R. (2003). Thermal remote sensing of urban climates. *Remote Sensing of Environment, 86*, 370-384.

Watson, K. (1992). Spectral ratio method for measuring emissivity. *Remote Sensing of Environment, 42*, 113-116.

APPENDIX A

MAP OF THE BUILDINGS ON CAMPUS

Figure A1 shows the locations of the buildings on campus. A list of buildings arranged by name and by number is presented in this appendix as well.

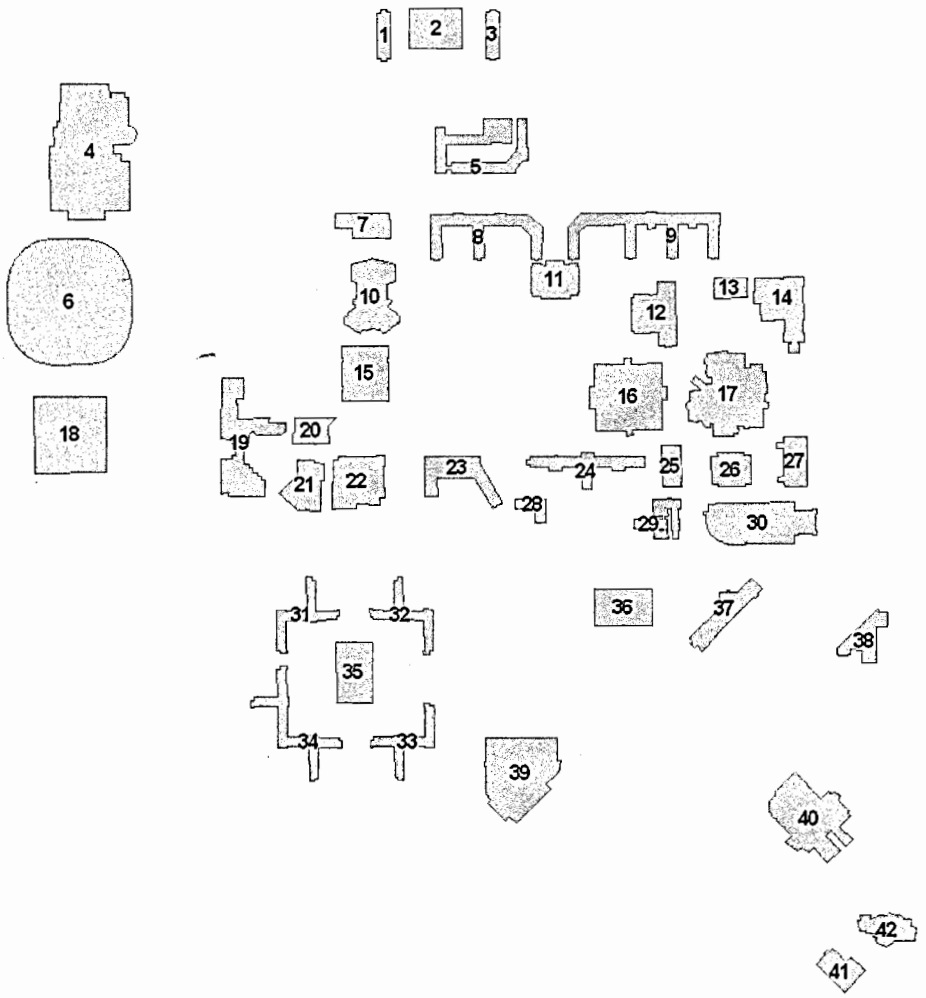

Figure A1. Map of the buildings on campus.

List of buildings on campus, arranged by number:

1 Bender Hall
2 Towers Center
3 Dancer Hall
4 Wellness Recreation Center
5 Campbell Hall
6 UNI Dome
7 Student Health Center
8 Lawther Hall
9 Bartlett Hall
10 Schindler Education Center
11 Commons
12 Innovative Teaching and Technology Center
13 Begeman Hall
14 Lang Hall
15 West Gymnasium
16 Library
17 Maucker Union
18 McLeod Center
19 Kamerick Art Building
20 Communication Arts Center
21 Strayer-Wood Theatre
22 Russell Hall
23 Curris Business Building
24 Baker Hall
25 Wright Hall
26 Sabin Hall
27 Seerley Hall
28 Facilities Services
29 Greenhouse Annex
30 McCollum Science Hall
31 Hagemann Hall
32 Rider Hall
33 Shull Hall
34 Noehren Hall
35 Redeker Center
36 Gilchrist Hall
37 Latham Hall
38 Biology Research Complex
39 Gallagher-Bluedorn Performing Arts Center
40 Industrial Technology Center
41 Business & Community Services
42 Center for Energy & Environmental Education

List of buildings on campus, arranged by alphabet:

24	Baker Hall
9	Bartlett Hall
13	Begeman Hall
1	Bender Hall
38	Biology Research Complex
41	Business & Community Services
5	Campbell Hall
42	Center for Energy & Environmental Education
11	Commons
20	Communication Arts Center
23	Curris Business Building
3	Dancer Hall
28	Facilities Services
39	Gallagher-Bluedorn Performing Arts Center
36	Gilchrist Hall
29	Greenhouse Annex
31	Hagemann Hall
40	Industrial Technology Center
12	Innovative Teaching and Technology Center
19	Kamerick Art Building
14	Lang Hall
37	Latham Hall
8	Lawther Hall
16	Library
17	Maucker Union
30	McCollum Science Hall
18	McLeod Center
34	Noehren Hall
35	Redeker Center
32	Rider Hall
22	Russell Hall
26	Sabin Hall
10	Schindler Education Center
27	Seerley Hall
33	Shull Hall
21	Strayer-Wood Theatre
7	Student Health Center
2	Towers Center
6	UNI Dome
4	Wellness Recreation Center
15	West Gymnasium
25	Wright Hall

APPENDIX B

TEMPERATURE HISTOGRAMS OF THE BUILDINGS ON CAMPUS

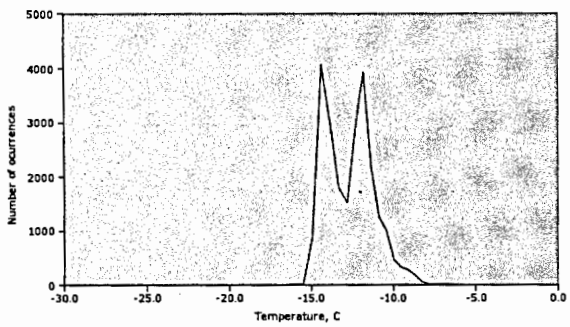

Baker Hall

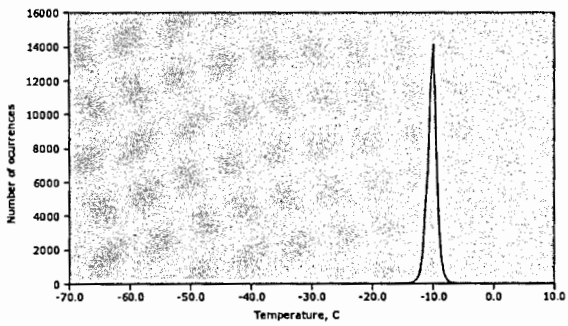

Bartlett Hall

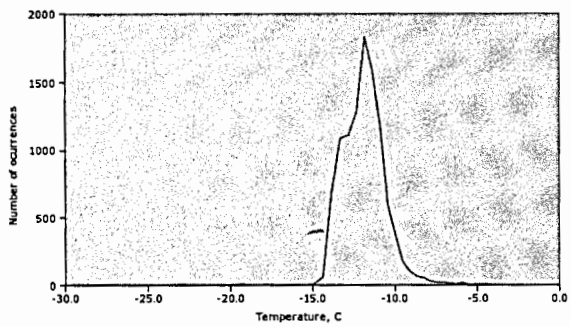

Bender Hall

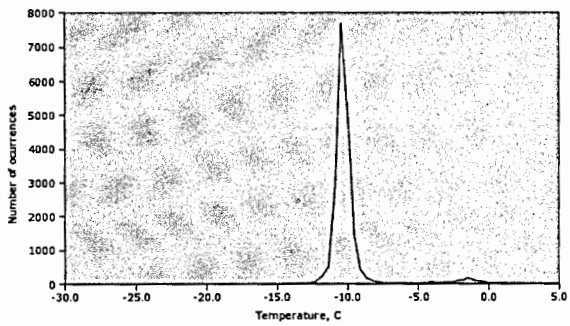

Biology Research Complex

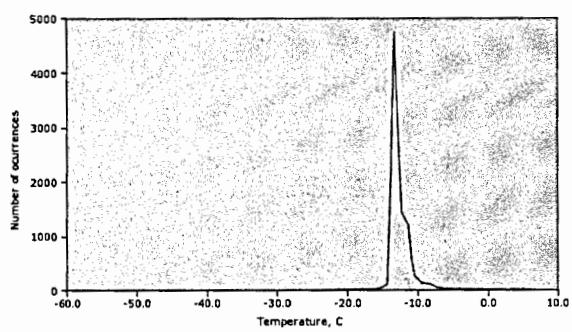

Business & Community Services

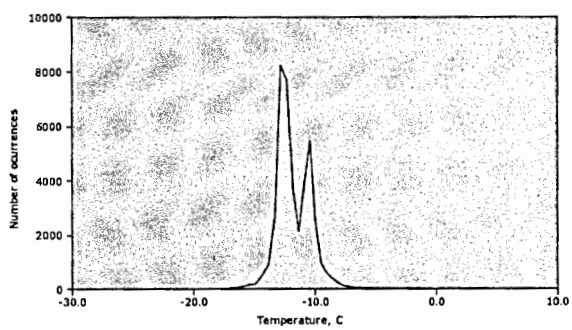

Campbell Hall

(figure continues)

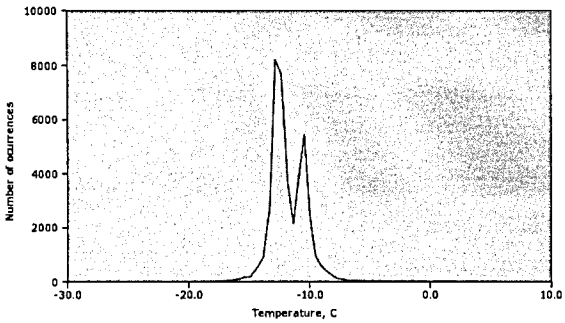

Center for Energy & Environmental Education

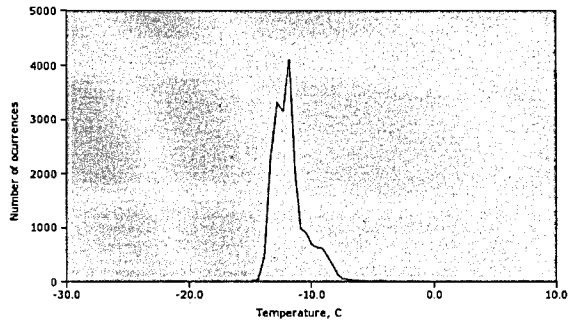

Commons

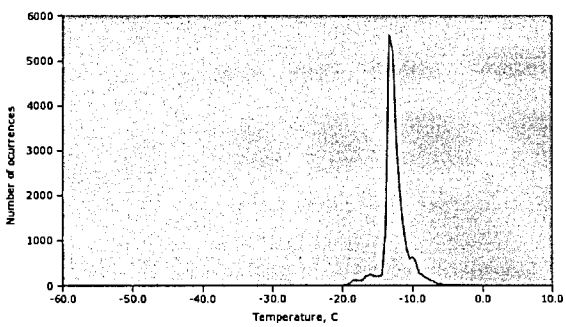

Communication Arts Center

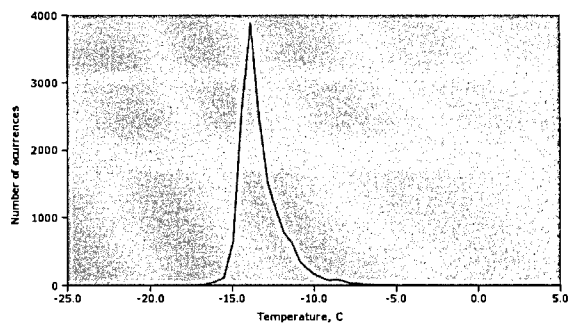

Curris Business Building

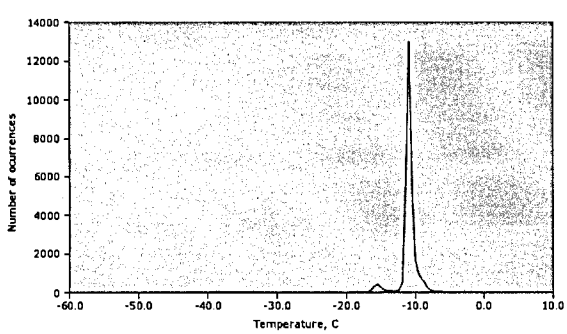

Dancer Hall

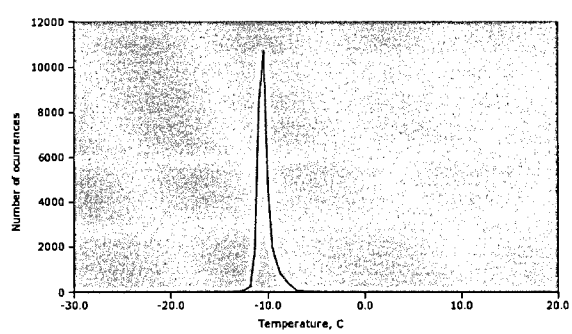

Facilities Services

(figure continues)

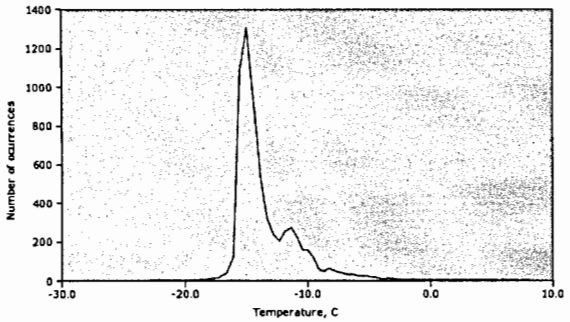

Gallagher-Bluedorn Performing Arts Center

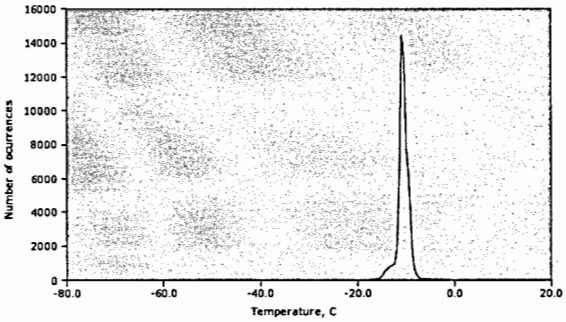

Greenhouse Annex

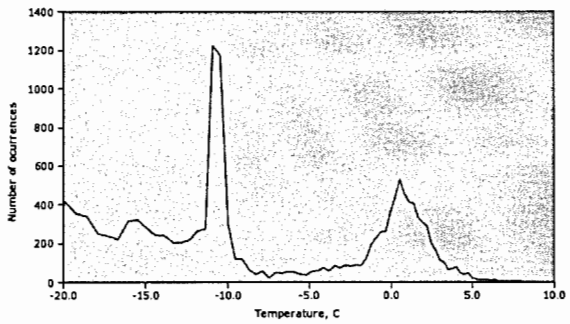

Hagemann Hall

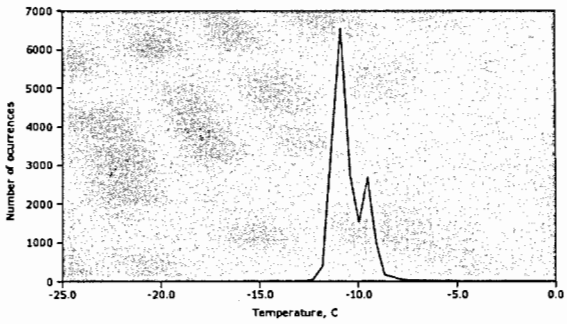

Industrial Technology Center

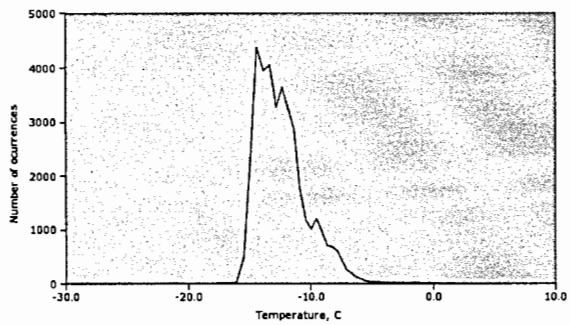

Innovative Teaching and Technology Center

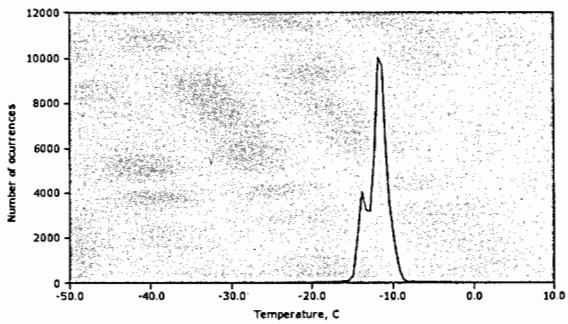

Kamerick Art Building

(figure continues)

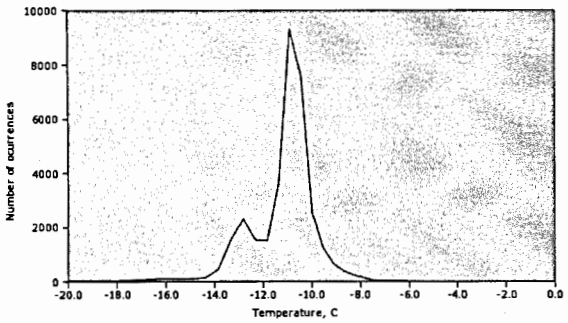

Lang Hall

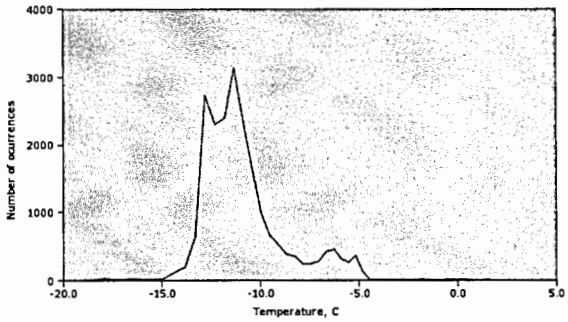

Latham Hall

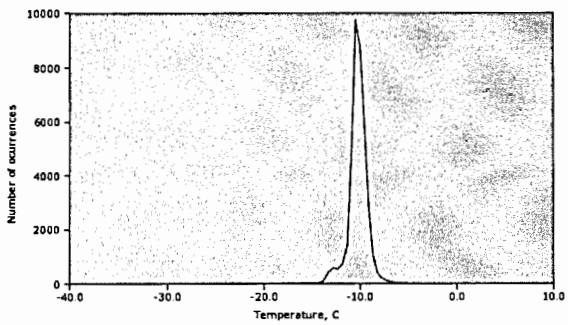

Lawther Hall

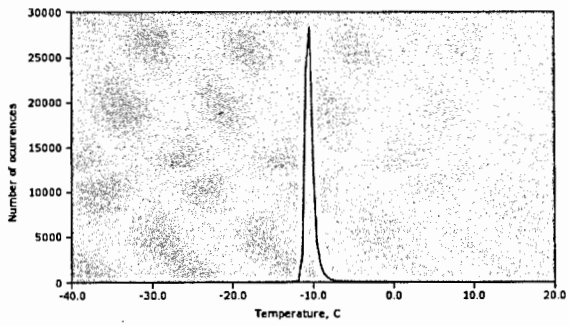

Library

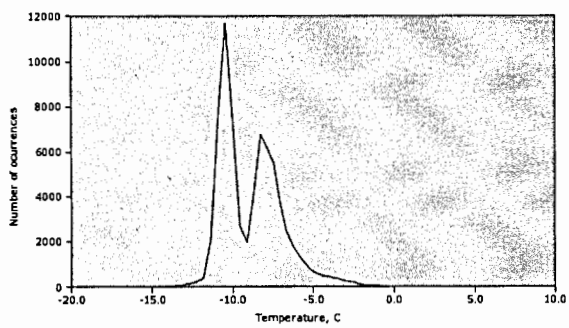

Maucker Union

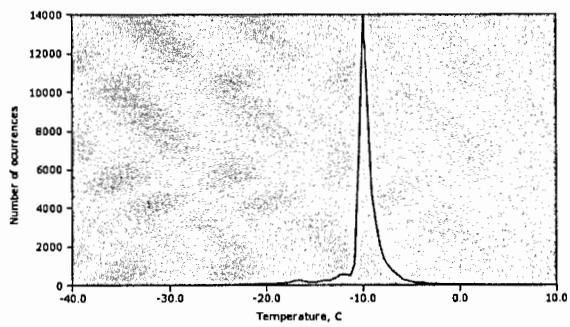

McCollum Science Hall

(figure continues)

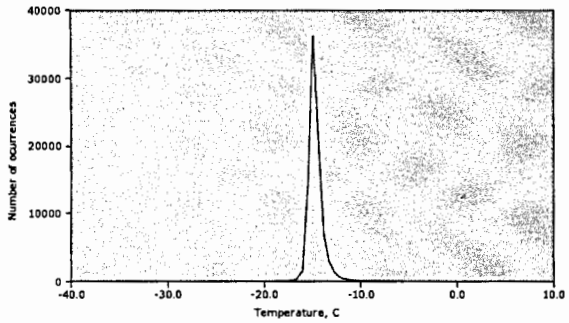

McLeod Center

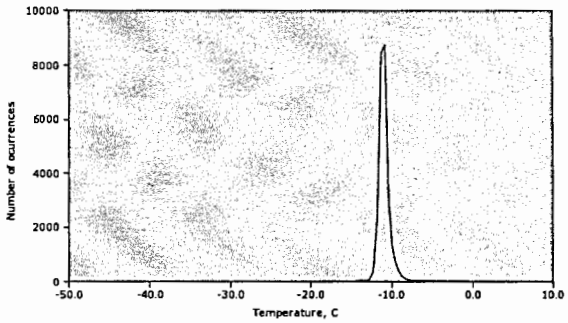

Noehren Hall

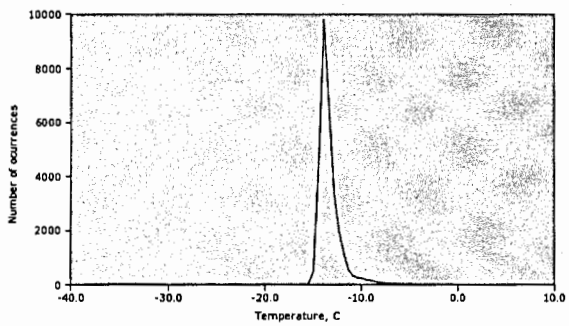

Redeker Center

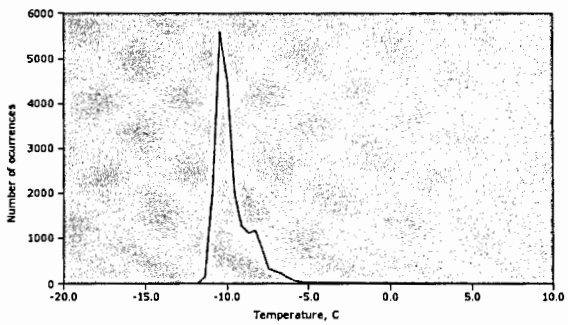

Rider Hall

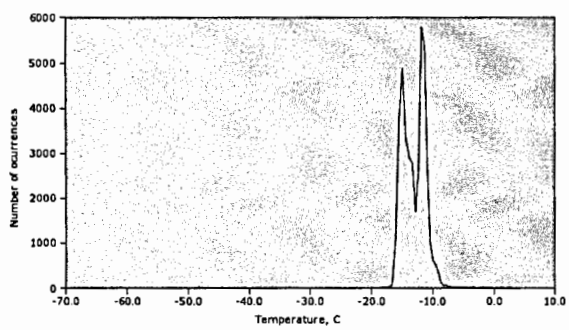

Russell Hall

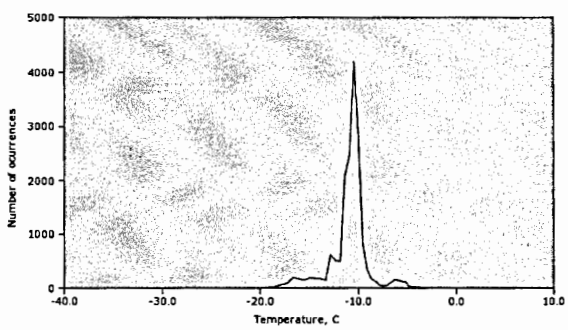

Sabin Hall

(figure continues)

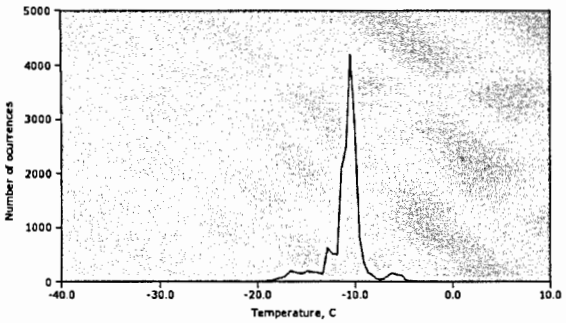

Schindler Education Center

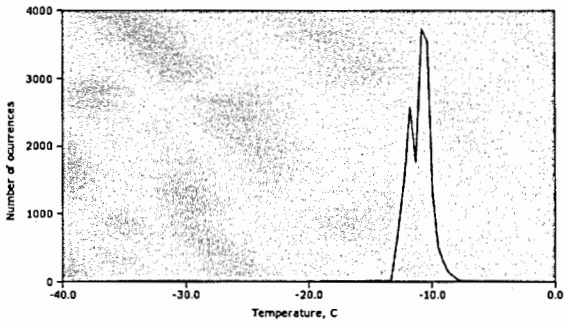

Seerley Hall

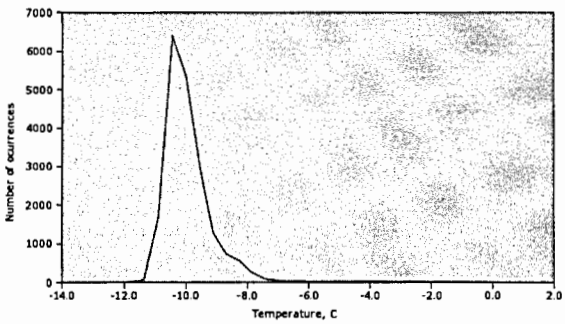

Shull Hall

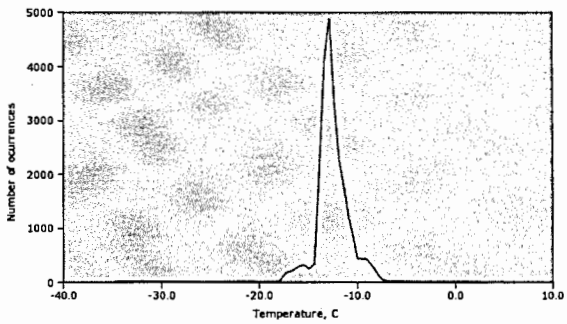

Strayer-Wood Theatre

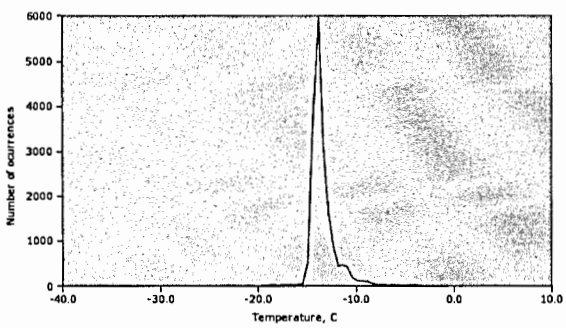

Student Health Center

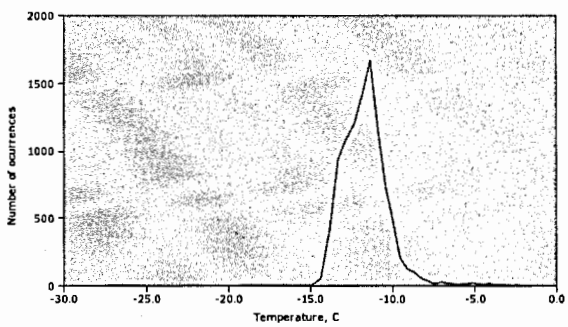

Towers Center

(figure continues)

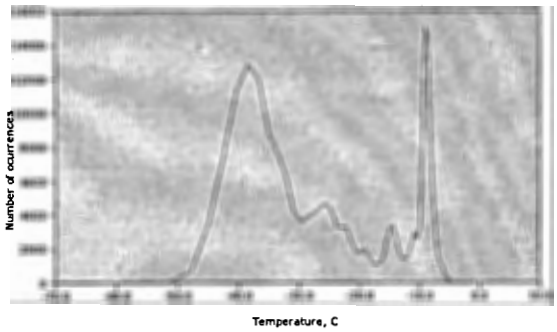

UNI Dome

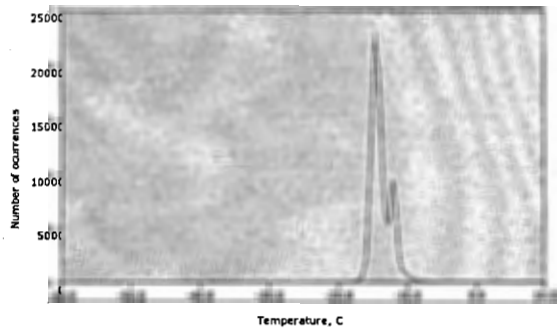

Wellness Recreation Center

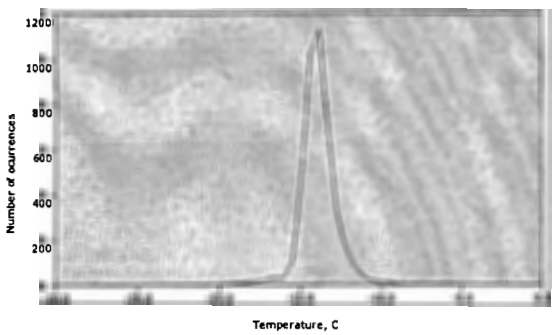

West Gymnasium

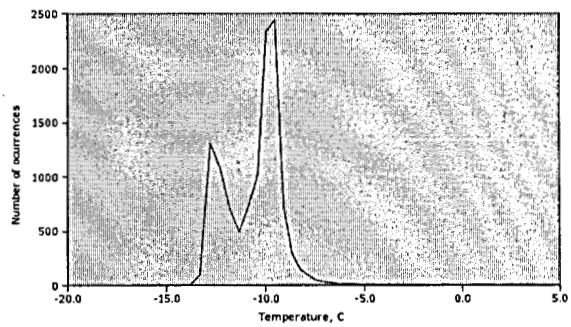

Wright Hall

Figure B1: Temperature histograms of the buildings on campus.